PHYSICAL REVIEW B VOLUME 52, NUMBER 2 1 JULY 1995-II

Transmission electron microscopy study of high-Zr-content lead zirconate titanate

Dwight Viehland
Department of Materials Science and Engineering, and the Materials Research Laboratory, University of Illinois, Urbana, Illinois 61801

(Received 6 January 1995)

Transmission electron microscopy studies have been performed on a series of $Pb(Zr_{1-x}Ti_x)O_3$ compositions for $0 \leq x \leq 0.2$. These studies revealed several important features of the phase transformational sequence. Locally ordered *R*-type and *M*-type oxygen octahedral rotations were found in the paraelectric state. Near the Curie temperature, a longer-range ordering of oxygen octahedral rotations was observed to develop. For $x \leq 0.05$, bright-field imaging and convergent beam electron-diffraction patterns revealed an intermediate ferroelectric phase with rhombohedral symmetry between low-temperature antiferroelectric orthorhombic and high-temperature paraelectric cubic states. This intermediate ferroelectric state was characterized by the presence of $\frac{1}{2}\langle 110 \rangle$ superlattice reflections, associated with ordered *M*-type oxygen octahedral rotations. Lattice imaging revealed nanosized domains which contained $\langle 110 \rangle$ structural modulations. With increasing Ti content, the intensity of the $\frac{1}{2}\langle 110 \rangle$ reflections was found to decrease. For $0.10 < x \leq 0.20$, only weak diffuse $\frac{1}{2}\langle 110 \rangle$ reflections were observed; however, on cooling strong $\frac{1}{2}\langle 111 \rangle$ reflections were found to develop. It is believed that a hierarchy of symmetries exists over a wide region of the rhombohedral ferroelectric phase field. A modification of the high-Zr-content end of the $Pb(Zr_{1-x}Ti_x)O_3$ phase diagram is then proposed to acount for this hierarchy.

I. INTRODUCTION

Lead zirconate (PZ) is the classic perovskite antiferroelectric. At high temperatures it is believed to possess prototypic cubic ($m3m$) symmetry. On cooling PZ is known to undergo two transformations which are close in temperature, one at ~230 °C and a second at ~220 °C. The temperature width of the intermediate region is known to be very sensitive to stoichiometry.[1–3] The low-temperature state has an orthorhombic structure, which is well established to an accuracy of 1 pm.[4,5] This structure possesses an antiparallel shift of Pb ions along the [110] resulting in antiferroelectricity. Jona *et al.*[4] assigned PZ to the space group *Pba*2 which is noncentrosymmetric, however, Fujishita and Hoshino proposed the centrosymmetric *Pbam*.[6] The structure of the intermediate-temperature state (220–230 °C) is considerably less well established. In fact, considerable controversy remains unresolved. Originally, it was believed that only one structural transformation occurred on cooling.[7] Later investigations revealed an intermediate tetragonal antiferroelectric phase, as shown in the classic $Pb(Zr_{1-x}Ti_x)O_3$ [PZT $(1-x)/x$] phase diagram for $x < 0.03$.[8] However, x-ray structural analysis has suggested that the intermediate state is rhombohedral ferroelectric.[9,10] It was suggested that the rhombohedral ferroelectric phase extends over from higher Ti contents towards PZ and that the tetragonal antiferroelectric phase in the PZT phase diagram is nonexistent. Evidence of an intermediate ferroelectric state exists from dielectric,[11] polarization,[12] and Raman[13] studies. Tanaka and Saito argued that the intermediate ferroelectric state has an orthorhombic symmetry by convergent beam electron diffraction (CBED) studies.[3] On the other hand, Fujishita and Hoshino believed that the intermediate state was antiferroelectric from neutron-diffraction investigations.[6] It remains unresolved whether the polar ordering in the intermediate phase region is ferroelectric or antiferroelectric, and whether the crystal structure is rhombohedral or orthorhombic or tetragonal.

It is quite clear that antiferroelectric transformations in PZ and PZT do not involve the condensation of a single zone-boundary polar phonon mode, as originally proposed by Kittel[14] and Cross.[15] The transition from the high-temperature cubic ($m3m$) structure to the orthorhombic antiferroelectric would seemingly involve at a minimum four phonon modes,[16] including a triply degenerate Γ_{25} *R*-point oxygen rotational mode, a zone-center Γ_{15} polar mode, a $(\frac{1}{2}\frac{1}{2}0)\pi/a$ Σ_3 mode, and a $(110)\pi/a$ M_5' mode. The softening of the zone-center Γ_{15} polar mode gives rise to a high permittivity near the dielectric maximum. The Σ_3 mode is the mode whose softening gives rise to the antipolar displacements of the Pb ions in the orthorhombic antiferroelectric (AFE_O) state with a phase of $(\uparrow\uparrow\downarrow\downarrow\uparrow\uparrow\downarrow\downarrow)$. The softening of the M_5' mode results in antiparallel displacements of Pb and Zr along the $[1\bar{1}0]$ with a phase $(\uparrow\downarrow\uparrow\downarrow)$. The softening of the Γ_{25} mode involves a counterclockwise rotation of successive oxygen layers along the [001].

Antiferroelectric transformations do not necessarily require an associated oxygen octahedral rotation, as the condensation of a simple zone-boundary polar phonon mode could occur. In principle, this is true, however, all known antiferroelectrics are not simple two-sublattice structures. Rather, a complex coupling between the Σ_3 mode and an oxygen rotation mode leads to antiferroelectricity.[17] Both the Σ_3 and Γ_{25} modes are known to be primary modes in the antiferroelectric orthorhombic state of PZ and PZT ($x < 0.05$).[16] In addition, antiferroelectric transformations in perovskites have been believed to be strongly displacive, with the nonexistence of local distortions and rotations above the transformation tempera-

0163-1829/95/52(2)/778(14)/$06.00

ture. However, there is no reason why local rotations associated with the Γ_{25} mode could not exist above the transformation temperature.

The purpose of this study was to investigate the intermediate state of PZ and the ferroelectric phase close to the antiferroelectric-ferroelectric phase boundary near the PZ end of the PZT crystalline solution series. Studies have been performed by hot- and cold-stage transmission electron microscopy (TEM) and Sawyer-Tower polarization (PE) measurements. It was anticipated that these studies might identify the structure and crystal symmetry of the intermediate phase region. In addition, it was anticipated that these studies might identify the role of the various oxygen rotational modes on the phase stability in the compositional range investigated.

II. EXPERIMENTAL TECHNIQUES AND PROCEDURES

Powders of lead zirconate titanate were prepared by a conventional mixed oxide method. Ceramic bodies were then formed by hot pressing at 1150 °C for 3 h, followed by an annealing at 1300 °C for 2 in a PbO excess environment. Detailed processing procedures have been published previously.[18]

These samples were examined using hot- and cold-stage TEM. TEM specimens were prepared by ultrasonically drilling 3-mm-diam discs which were mechanically polished to a thickness of $\sim 100\ \mu$m. The center portions of these discs were then further ground by a dimpler to $\sim 10\ \mu$m, and argon-ion-milled to perforation. Specimens were coated with carbon before examination. The TEM studies were done on a Phillips EM-420 microscope operating at an accelerating voltage of 120 kV, using double-tilt hot and cold stages.

The polarization electric-field behavior (PE) was characterized using a computer-controlled modified Sawyer-Tower circuit. Specimens were immersed in a silicon oil bath within a test chamber which could be operated between 25 and 250 °C. All PE curves were measured at a frequency of 50 Hz.

III. SOFT MODES AND RESULTANT SUPERLATTICE REFLECTIONS

The PE-FE transformation in rhombohedral PZT occurs due to the condensing of a Brillouin zone-center Γ_{15} polar phonon mode.[16] The softening of the Γ_{15} mode results in parallel displacements of the B-site cations along the $\langle 111 \rangle$. Antiferroelectricity in PZT occurs due to a condensation of a $(\frac{1}{2}\frac{1}{2}0)(\pi/a)\Sigma_3$ mode. The Σ_3 mode contains antiparallel Pb cation displacement in the $\langle 001 \rangle$ plane when referenced to the paraelectric (cubic) phase. The softening of this mode results in the appearance of $\frac{1}{4}\langle 110 \rangle$ superlattice reflections in the electron-diffraction patterns.

The softening of the Γ_{25} mode results in the opposite rotations of successive oxygen layers along the [001].[19] The primitive unit cell is doubled along the [001]. In addition, the cog-wheel-like rotations of the nearest-linked oxygen octahedron in the (001) plane double the primitive unit cell along the [100] and [010]. Throughout following discussions, unless specifically stated otherwise, all $\langle hkl \rangle$ will be referred to pseudocubic ones. The condensation of the Γ_{25} mode results in the appearance of $\frac{1}{2}\langle 111 \rangle$ superlattice reflections (F spots).[17] These oxygen rotations will be referred to as the R-point or R-type tilted state throughout this paper. Since the Γ_{25} mode at the R point of the Brillouin zone is triply degenerate, transformations associated with it can occur in different ways depending on various linear combinations of degenerate modes. Each type of linear combination is known to produce $\frac{1}{2}\langle 111 \rangle$ superlattice reflections. Condensation of a single Γ_{25} mode in $SrTiO_3$ near 110 K results in oxygen rotations about the [001] stabilizing an oxygen framework with tetragonal symmetry.[20] The condensation of a linear combination of two Γ_{25} modes is known to exist in the AFE_O state of $PbZrO_3$.[16] In this case, the composed oxygen rotations occur about the $\langle 110 \rangle$, stabilizing an oxygen framework with orthorhombic symmetry. The transformation between the low-temperature and high-temperature rhombohedral ferroelectric ($FE_{R(HT)}$ and $FE_{R(LT)}$, respectively) phases in $Pb(Zr_xTi_{1-x})O_3$ is an example of a transformation driven by the condensation of a linear combination of all three Γ_{25} modes. The composed oxygen rotations occur about the $\langle 111 \rangle$, stabilizing an oxygen framework with rhombohedral symmetry.[19]

Another type of oxygen rotation which can occur is due to an instability of the M_3 mode at $\mathbf{q}=(110)(\pi/a)$ or the M point of the Brillouin zone boundary. The existence of a soft M_3 mode in PZT has been suggested, but not extensively investigated.[6] The softening of an M_3 mode results in the rotations of successive oxygen layers along the [001] in the same direction[19] (referred to as the M-point or M-type tilted state throughout this paper). Consequently, the condensation of an M_3 mode does not double the primitive unit cell along the [001]. However, the coplanar cog-wheel-like oxygen rotations double the primitive unit cell along the [100] and [010] axes, producing a structure with tetragonal symmetry. As a consequence, $\frac{1}{2}\langle 110 \rangle$ superlattice reflections can be expected to appear in the electron-diffraction patterns.

IV. RESULTS AND DISCUSSIONS

A. $PbZrO_3$

1. Ordered and locally ordered oxygen rotations

Figure 1(a) shows the room-temperature bright-field image of PZ. 90° antiferroelectric domains can be seen in this figure. A $\langle 001 \rangle$ selected area electron-diffraction (SAED) pattern is shown in Fig. 1(b). In this figure, $\frac{1}{4}\langle 110 \rangle$ superlattice reflections can be seen along two dimensions. The two-dimensionality arises due to neighboring AFE domains which have the same $\langle 001 \rangle$ orientation but are rotated by 90° with respect to each other. The superlattice reflections reveal the quadrupling of the unit cell along the $\langle 110 \rangle$, associated with the soft Σ_3 mode and the antiparallel alignment of dipole moments along the $\langle 110 \rangle$ axis. It should be mentioned that this

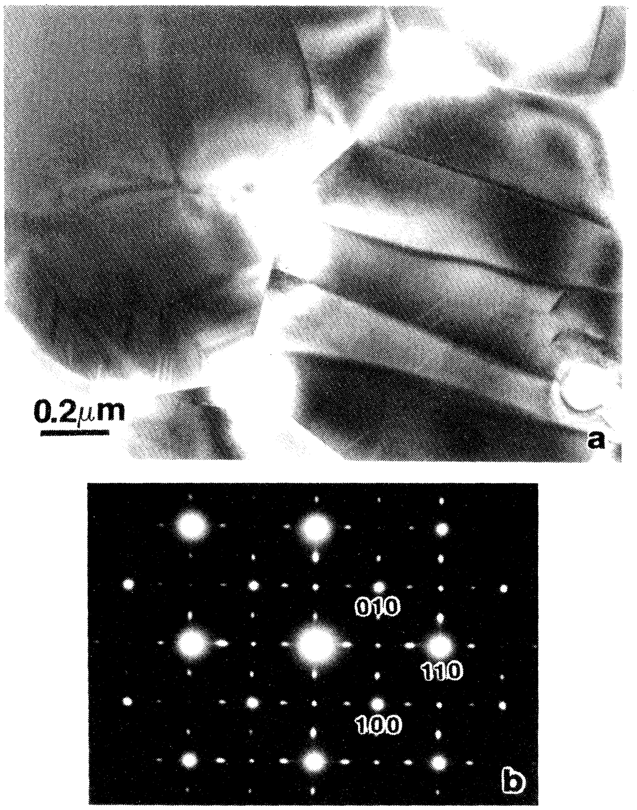

FIG. 1. Room-temperature TEM results for PZ. (a) Bright-field image, and (b) ⟨112⟩ SAED pattern.

antiparallel alignment does not correspond to a two-sublattice model involving the condensation of a single zone-boundary polar phonon mode. The c/a ratio was calculated from the ⟨100⟩ SAED pattern and was found to be equal to ~ 0.987, in agreement with previous reports.[21] These results show that the room-temperature structure of PZ is a commensurate antiferroelectric orthorhombic (AFE$_O$), as is well known.

Figures 2(a)–2(f) illustrate the temperature dependence of the ⟨112⟩ SAED patterns at temperatures of 20, 200, 210, 225, 320, and 530 °C, respectively. $\frac{1}{4}$⟨110⟩ structural modulations indicative of the commensurate AFE$_O$ state can be seen between 20 and 210 °C [Figs. 2(a)–2(c)]. The AFE$_O$ structure remained commensurate until a transformation near 220 °C, which is in agreement with the temperature previously reported for the intermediate phase region between the AFE$_O$ and paraelectric (PE) states. $\frac{1}{2}$⟨111⟩ superlattice reflections were also present in the AFE$_O$ state [marked by F in Fig. 2(a)]. The transformation into the intermediate state was characterized by the appearance of $\frac{1}{2}$⟨110⟩ superlattice reflections, as indicated in Fig. 2(d) by an arrow. $\frac{1}{2}$⟨111⟩ superlattice reflections were also present in the intermediate state. No significant change in intensity of the $\frac{1}{2}$⟨111⟩ reflections was observed at the transformation between the AFE$_O$ and intermediate states.

The transformation to the paraelectric state was characterized by the development of diffuseness in the $\frac{1}{2}$⟨110⟩ and $\frac{1}{2}$⟨111⟩ superlattice reflections [see Fig. 3(e)]. Weak diffuse reflects were apparent until temperatures above 500 °C [Fig. 3(f)]. These results indicate that the transformation from the PE state to the intermediate state does not occur directly from an ideal $m3m$ symmetry. Rather, it would appear that the oxygen octahedron remain locally tilted to temperatures much greater than that of the AFE$_O$-intermediate-PE transformational sequence. Recently, the rotation angle of the oxygen tilt structure has also been found to be nonzero far above the antiferrodistortive transformation temperature for NaTaO$_3$.[22] No anomaly in the rotation angle was observed near the antiferroelectric transformation, rather the angle slowly decreased with increasing temperature. In consideration of the results presented in this section, it would seem apparent that the antidistortive transformation in many perovskites is not accompanied by a condensation of an oxygen octahedral rotation mode, rather the softening of the zone-boundary Σ_3 mode may occur within an already locally tilted oxygen framework.

$\frac{1}{2}$\{110\} superlattice reflections have previously been detected in the intermediate FE phase (228–235 °C) of PZ neutron diffraction.[6] Fujishita and Hoshino believed that the $\frac{1}{2}$\{110\} reflections were due to a softening of the M'_2, M'_3, and M'_5 modes, which involve antiparallel displacements of cations and oxygens.[6] However, the presence of diffuse $\frac{1}{2}$\{110\} reflections far into the PE state [Fig. 2(a)] excludes the possibility that cation displacements associated are the origin of the observed structural ordering. Randall *et al.*[23] have previously reported the presence of weak $\frac{1}{2}$\{110\} reflections by SAED over a wide temperature range in Pb-based perovskites. They attributed the $\frac{1}{2}$\{110\} reflections to short-range A-site vacancy ordering. If this is the case for PZ, the intensity of the $\frac{1}{2}$\{110\} reflections should be temperature independent below the ordering temperature, as a change in the degree of ordering would require lattice diffusion. However, the results for PZ revealed a transition from $\frac{1}{2}$\{110\} to $\frac{1}{2}$\{111\} reflections on cooling. This transition excludes the possibility of vacancy ordering as the origin of the $\frac{1}{2}$\{110\} structural ordering. In consideration of the presence of diffuse $\frac{1}{2}$\{110\} reflections in the PE state, the transition between $\frac{1}{2}$\{110\} and $\frac{1}{2}$\{111\} reflections on cooling, and the exclusion of other obvious possibilities, we believe that the origins of $\frac{1}{2}$\{110\} reflections is due to a soft M_3 oxygen rotational mode. Glazer and Megaw[24] have previously shown that the cubic to tetragonal transformation at 640° C for NaNbO$_3$ occurs due to the condensation of this mode, resulting in $\frac{1}{2}$\{110\} reflections.

Observation of diffuse $\frac{1}{2}$⟨111⟩ and $\frac{1}{2}$⟨110⟩ superlattice reflections to high temperatures indicates the coexistence of both R-type and M-type oxygen rotations over a wide temperature range. The diffuseness of the reflection intensity above the transformation indicates that the oxygen rotations are only locally ordered. Diffuse $\frac{1}{2}$⟨111⟩ superlattice intensity has recently been observed to high temperatures in antiferroelectric PZST and PLZT ceramics.[25,26] Impurities may influence the degree of local tilting of the oxygen octahedra in PZ, however, intrinsic

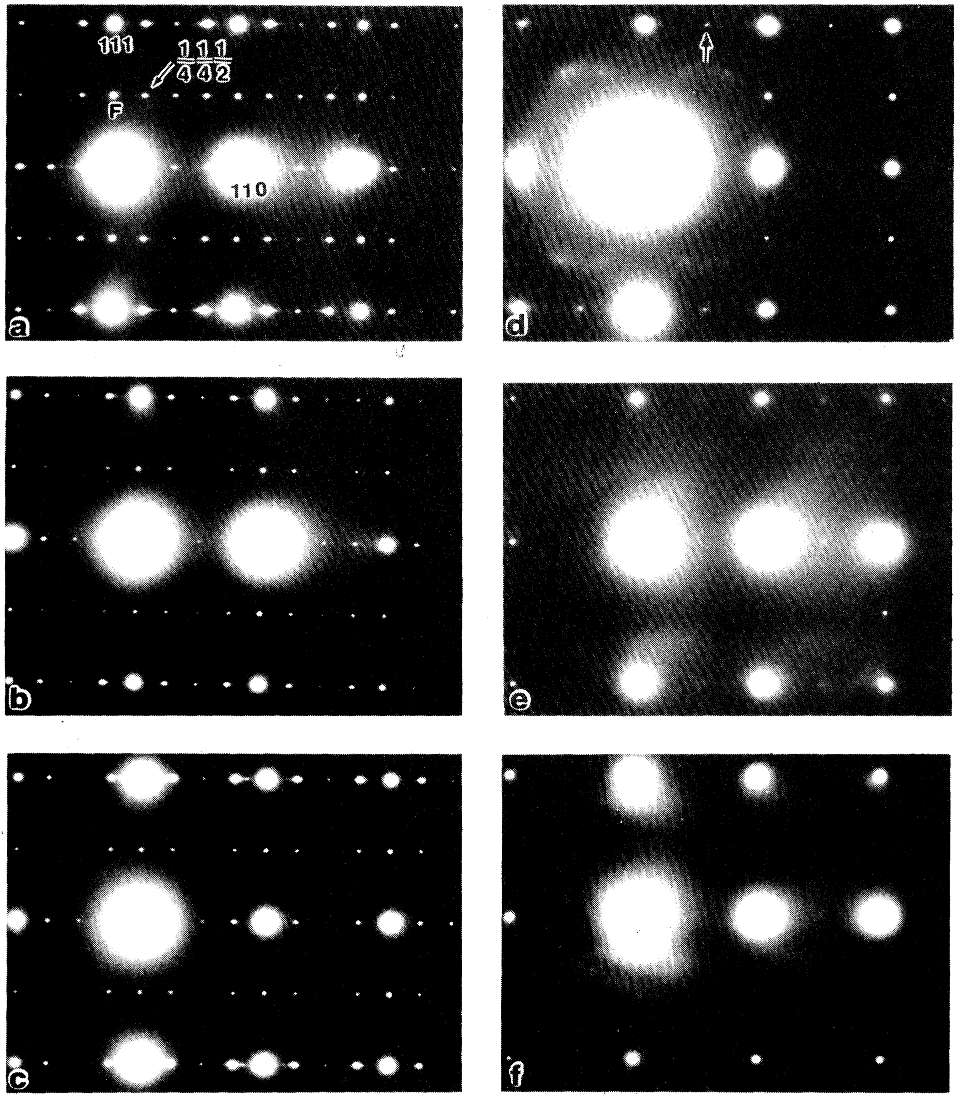

FIG. 2. $\langle 112\rangle$ SAED patterns of PZ at temperatures (a) 20 °C, (b) 200 °C, (c) 210 °C, (d) 225 °C, (e) 320 °C, and (f) 530 °C.

diffuse $\frac{1}{2}\langle 111\rangle$ and $\frac{1}{2}\langle 110\rangle$ reflections were evident in undoped ceramics and single crystals to a temperature far above the antidistortive transformation. Clearly, locally ordered intrinsic oxygen rotations exist far into the cubic phase for PZ. These locally ordered rotations may influence the evolution of the antiferroelectric transformation and should be taken into account in order to better understand antidistortive phase transformations. The results presented here may indicate that the antiferroelectric transformation in Pb-based perovskites has some characteristics of an order-disorder transformation, within rotated oxygen octahedrons.

At the transformation into the intermediate phase region on cooling, a distinct sharpening of the $\frac{1}{2}\langle 110\rangle$ superlattice reflections was observed. In the paraelectric state, the oxygen rotations may be only locally ordered, however at the transformation temperature into the intermediate phase region the rotations undergo a significant increase in their degree of long-range order. The fact that the long-range ordering of the oxygen octahedra was coincidental with the transformation into the intermediate state indicates a coupling between the Γ_{15} zone-center and M_3 oxygen rotational modes. This coupling would seemingly stabilize the intermediate phase region, as below the intermediate AFE_O transformation only $\frac{1}{2}\langle 111\rangle$ reflections remained. A coupling between the Σ_3 zone-boundary and Γ_{25} oxygen rotational modes would seemingly stabilize the AFE_O state. An anharmonic coupling of the Σ_3 and Γ_{25} modes is known to exist, resulting in the formation of $\langle \frac{1}{4}\frac{1}{4}\frac{1}{2}\rangle$ structural modulations, as confirmed by $\langle \frac{1}{4}\frac{1}{4}\frac{1}{2}\rangle$ superlattice reflections in the $\langle 112\rangle$ SAED patterns observed in this study [marked in Fig. 2(a)]. In consideration that antiferroelectric states are known to be only marginally stable over ferroelectric states, this anharmonic coupling may be responsible for the stability of antiferroelectricity in Pb-based perovskites.

Figure 3(a)–3(f) show $\langle 001\rangle$ SAED patterns at various temperatures on heating and subsequent recooling. Pat-

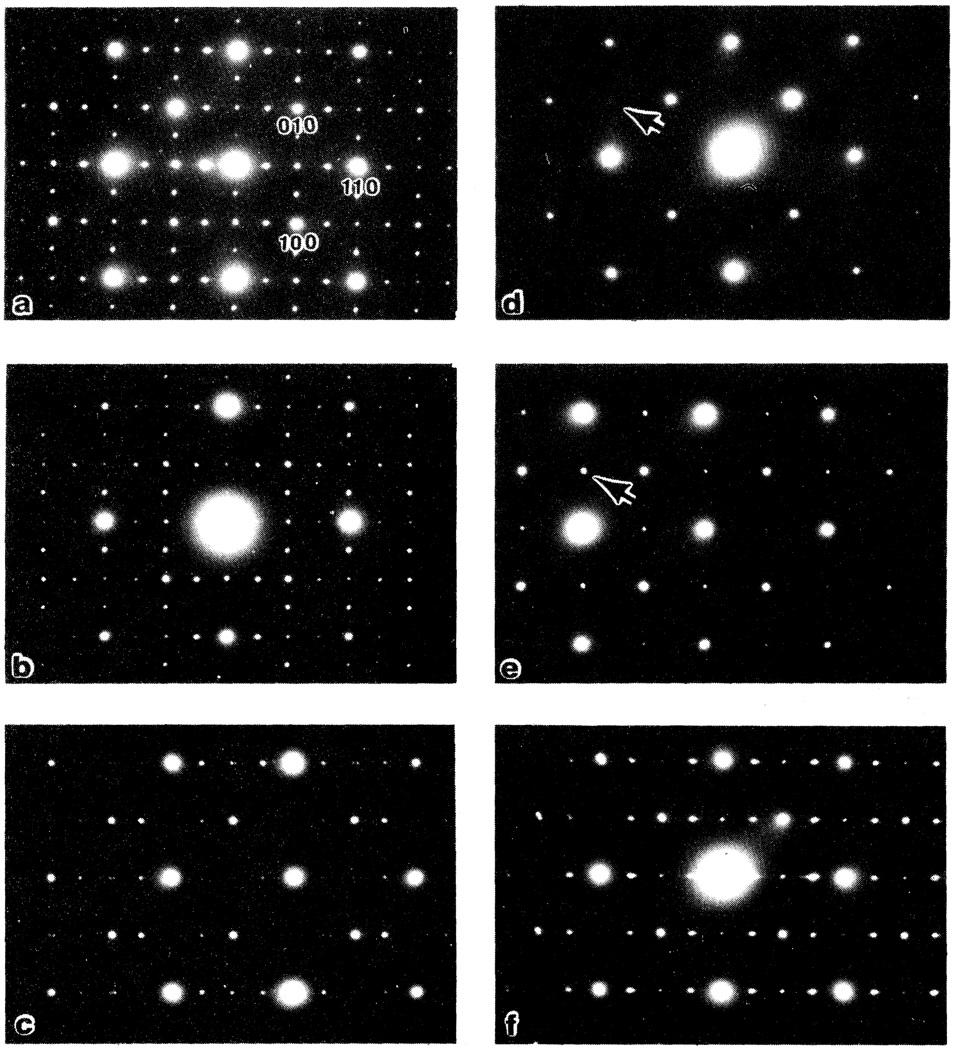

FIG. 3. ⟨001⟩ SAED patterns of PZ on heating and subsequent cooling (a) 20 °C, (b) 170 °C, (c) 220 °C, (d) 240 °C, (e) 200 °C, and (f) 20 °C.

terns are shown at consecutive temperatures of 20, 170, 220, 240, 200, and 20 °C, respectively. $\frac{1}{4}\langle 110\rangle$ superlattice reflections are clearly evident between 20 and 170 °C [Figs. 3(a) and 3(b)], as previously shown in the ⟨112⟩ SAED patterns given in Figs. 2(a) and 2(b). With increase of temperature, the intensity of the superlattice reflections decreased. On further increase of the temperature to the paraelectric state [Fig. 3(d)], only diffuse $\frac{1}{2}\langle 110\rangle$ superlattice reflections were observed. However on recooling, different trends were observed. Strong $\frac{1}{2}\langle 110\rangle$ superlattice reflections were obvious (with no indications of $\frac{1}{4}\langle 110\rangle$ reflections) until temperatures below 200 °C [Fig. 3(e)], indicating a thermal hysteresis in the intermediate phase region. $\frac{1}{4}\langle 110\rangle$ reflections were found to develop on further cooling, as illustrated in Fig. 3(f).

Figure 4 shows the dielectric constant and tanδ measured at 100 kHz as a function of temperature for PZ on heating and cooling measurements. Inspection of the dielectric data reveals two dielectric anomalies, which are close in temperature. A principle dielectric maximum of ~6000 can be seen near 238 °C on heating and 233 °C on cooling, in agreement with accepted values. A secondary anomaly can be seen just below the principle peak. These results indicate a sequence of two transformations on cooling. The temperature stability range of the intermediate state can be seen to exhibit significant thermal hysteresis between heating and cooling, indicating a region of metastability. The temperature widths were ~1–2 °C on heating and ~15 °C on cooling. In the cooling mode, the dielectric loss factor can be seen to be highest in the temperature range of the intermediate state. A possible interpretation of these results is that the intermediate phase region is ferroelectric, as ferroelectric states are known to have significantly higher losses than antiferroelectric.[27,28]

These results indicate a region of metastability between the AFE_O and intermediate states between heating and cooling, which is clearly associated with the *M*-type oxygen rotations. Evidence of metastability in this temperature range has also been found from dielectric property studies. On heating, ordered *M*-type oxygen rotations may be slow to develop within the AFE_O state, tending to stabilize the AFE_O state to higher temperatures.

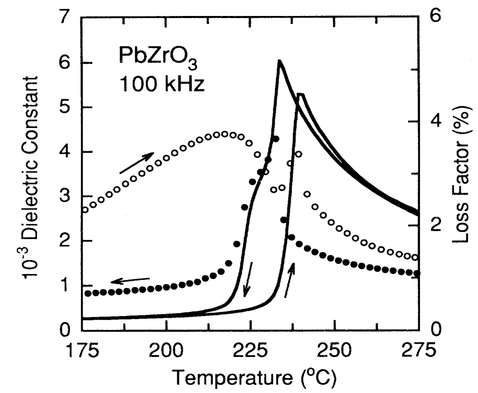

FIG. 4. Dielectric constant (solid lines) and loss factor (dashed lines) for PZ on heating and cooling measurements, respectively.

However, locally ordered M-type oxygen rotations may develop relatively easily in the paraelectric state. On cooling to the intermediate phase region, the oxygen rotations then order with the condensation of a polar phonon mode. Consequently, strong $\frac{1}{2}\langle 110\rangle$ reflections are observed on cooling into the intermediate phase region. On further cooling, the ordered M-type oxygen rotations may be slow to disappear at the intermediate AFE_O transformation, tending to stabilize the intermediate state. The implication is that the M-type oxygen rotational system may be able to metastably trap an intermediate ferroelectric phase region.

2. *Nature of intermediate phase region*

Figure 5 shows a bright-field image at 225 °C which was taken after cooling through the Curie point. A $\langle 001\rangle$ SAED pattern is shown in the inset, which clearly reveals only $\frac{1}{2}\langle 110\rangle$ superlattice reflections. The bright-field image reveals ferroelectric domain patterns which are similar to those observed in rhombohedral ferroelectric PZT.[29] The domains were found to be sensitive to orientation and to exhibit a high mobility under electron beam illumination. Clearly, the intermediate phase region is ferroelectric. On cooling below 200 °C, the ferroelectric domain patterns suddenly disappeared and antiferroelectric domains and $\frac{1}{4}\langle 110\rangle$ superlattice reflections appeared.

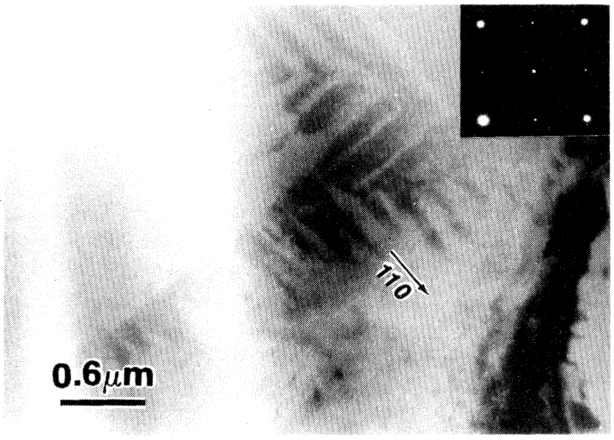

FIG. 5. Bright-field image of PZ in the intermediate phase region (225 °C).

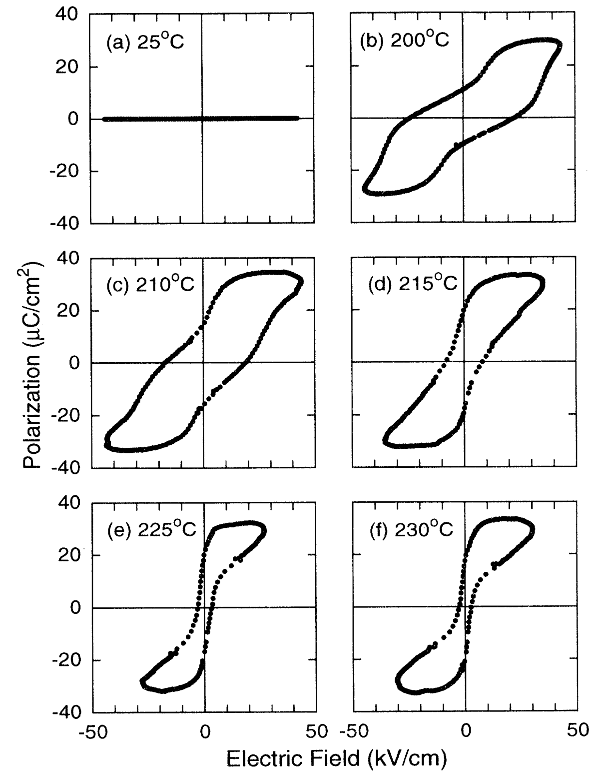

FIG. 6. Dielectric hysteresis loops of PZ at temperatures (a) 25 °C, (b) 200 °C, (c) 210 °C, (d) 215 °C, (e) 225 °C, and (f) 230 °C.

The temperature dependence of the polarization electric field (PE) behavior is illustrated in Figs. 6(a)–6(f) at temperatures of 25, 200, 210, 215, 225, and 230 °C, respectively. In the temperature range between 200 and 210 °C, PE curves with characteristics of double hysteresis loops were observed suggestive of an electrically induced antiferroelectric-ferroelectric transformation. However, at temperatures between 210 and 235 °C, PE curves typical of that of a ferroelectric were observed, which is in agreement with the TEM result that revealed ferroelectric domains in the same temperature range. The magnitude of the saturation polarization, remanent polarization, and coercive field were approximately 33 $\mu C/cm^2$, 20 $\mu C/cm^2$, and 10 kV/cm, respectively.

Figures 7(a)–7(c) illustrate [001] zone axis CBED patterns obtained from the same region at the sequential temperatures of 20, 380, and 200 °C. These temperatures correspond to the AFE_O, PE, and intermediate ferroelectric phase regions, respectively. At 20 °C [Fig. 7(a)], the CBED pattern possessed a 2-mm diffraction symmetry. In this pattern, the two-fold rotation axis was parallel to

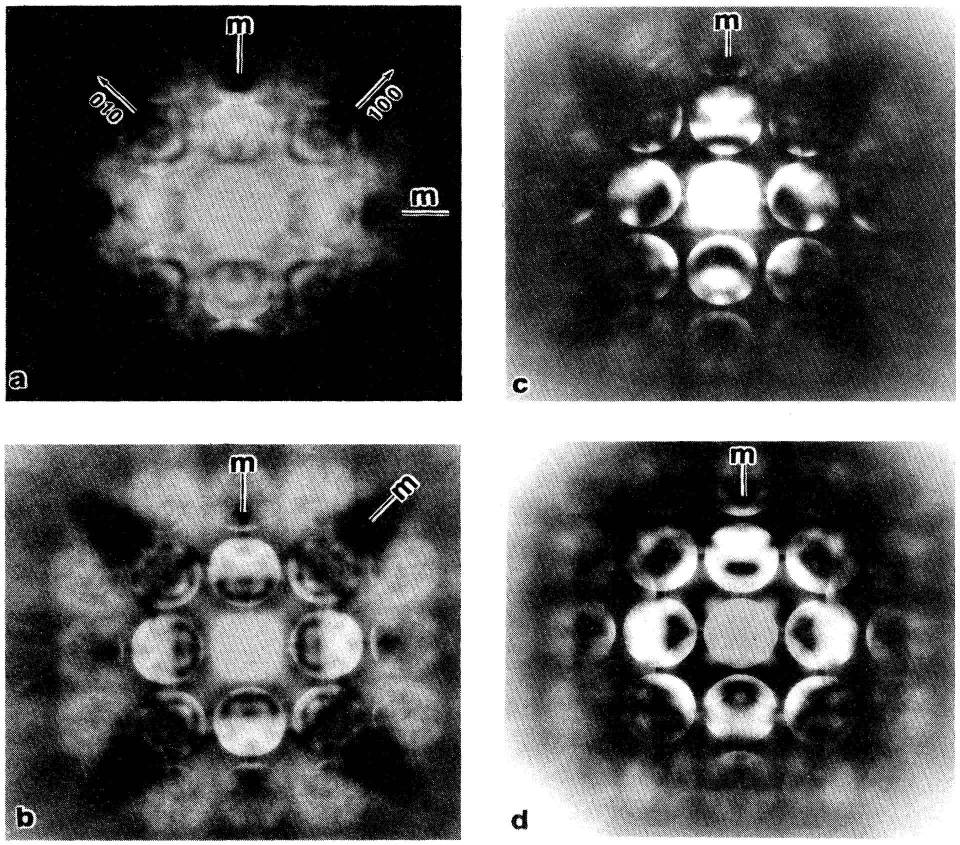

FIG. 7. [001] zone-axis convergent beam electron-diffraction patterns for PZ at various temperatures. (a) 20 °C, (b) 380 °C, (c) 200 °C, and (d) PZT 65/35 at room temperature (shown for comparisons).

the [001] and the two mirror planes were perpendicular to each other and parallel to the [110] and [$1\bar{1}0$]. These symmetry patterns are typical of that of an orthorhombic structure. At 380 °C [Fig. 7(b)], 4-mm diffraction symmetry can be seen. In this pattern, the four-fold rotation axis is parallel to the [001] and the two mirror planes are parallel to the [100] and [110]. These symmetry patterns are typical of that of a cubic structure. In the intermediate phase region [Fig. 7(c)], only one mirror plane can be seen which is parallel to the [110]. In the ferroelectric rhombohedral state, the projection of [111] cation displacements onto the pseudocubic a-b plane leads to a single mirror plane parallel to the [110] when viewed along the [001] axis, as shown in the [001] CBED pattern for PZT 65/35 [Fig. 7(d)]. Clearly, the intermediate ferroelectric phase region in PZ has rhombohedral symmetry.

The stability of the intermediate phase region has been reported to be dependent on "impurity" content.[2,9] Impurities may relax the oxygen framework, preferentially favoring one of the oxygen tilt systems. Consequently, the temperature range, structure, and polar ordering of the intermediate phase region may be strongly dependent on small dopants. We believe that this effect might help explain the inconsistencies reported in the literature concerning the intermediate phase region. Recent investigations in our laboratories have shown that addition of 2 at. % La to PZ results in the stabilization of an incommensurate antiferroelectric state in the intermediate-temperature region. The results from this investigation will be reported separately.[30]

B. $\mathrm{Pb(Zr_{0.95}Ti_{0.05})O_3}$

1. Electron-diffraction studies

Figures 8(a) and 8(b) show two bright-field images taken at room temperature for PZT 95/5. Figure 8(a) reveals a typical microstructure for the dominate phase of the specimen. Normal rhombohedral ferroelectric domain patterns were evident. A representative microstructure for the minor phase is shown in Fig. 8(b). Figure 8(b) clearly shows the coexistence of ferroelectric and antiferroelectric domain structures. The domain patterns are typical of those observed in the antiferroelectric orthorhombic (AFE_O) phase of PZ. In this region structural modulation along $\langle 110 \rangle$ are obvious.

$\langle 001 \rangle$ and $\langle 110 \rangle$ SAED patterns which were taken from grains in Fig. 8(a) are shown in Figs. 8(c) and 8(d), respectively. The patterns in these figures clearly reveal the existence of $\frac{1}{2}\langle 110 \rangle$ superlattice reflections as arrowed, which are similar to those observed in the intermediate ferroelectric phase of PZ. The existence of $\frac{1}{2}\langle 110 \rangle$ superlattice reflections was found to be characteristic of the ferroelectric phase for PZT 95/5. $\langle 001 \rangle$ and $\langle 110 \rangle$ SAED patterns which were taken from an antiferroelectric region in Fig. 8(b) are shown in Figs. 8(e) and 8(f), respectively. Figure 8(e) reveals the existence of

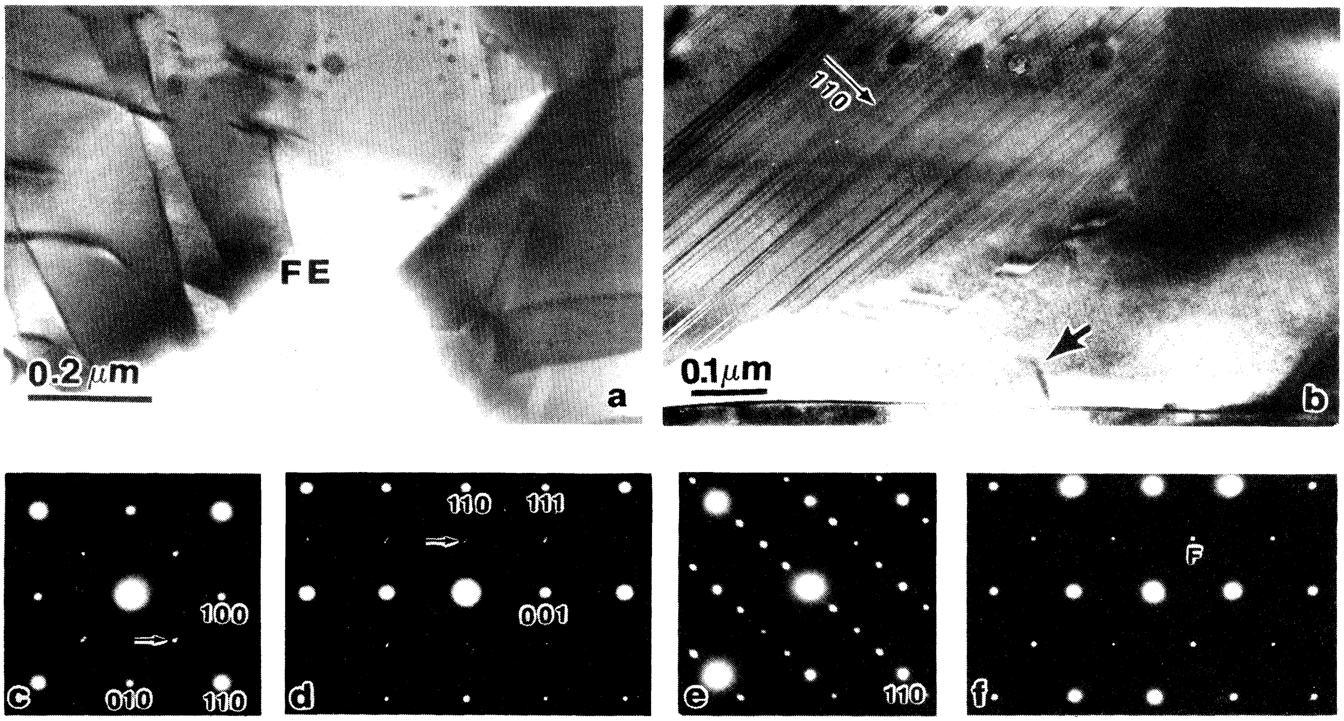

FIG. 8. Bright-field image and diffraction patterns of PZT 95/5 at 25 °C (a) dominant FE phase, (b) minor AFE phase, (c) ⟨001⟩ SAED pattern of the FE phase, (d) ⟨110⟩ SAED patterns of the FE phase, (e) ⟨001⟩ SAED pattern of the AFE phase, and (f) ⟨110⟩ SAED pattern of the AFE phase.

$\frac{1}{4}\langle 110\rangle$ superlattice reflections, which were isomorphous with that of AFE$_O$ PZ shown above. Figure 8(f) reveals the existence of $\frac{1}{2}\langle 111\rangle$ superlattice reflections, no $\frac{1}{2}\langle 110\rangle$ reflections were detected. These results illustrate that the dominate phase of PZT 95/5 is ferroelectric. The presence of $\frac{1}{2}\langle 110\rangle$ superlattice reflections indicate the presence of a soft M_3 oxygen rotational mode. The structure of the ferroelectric phase is isomorphous with that of the intermediate ferroelectric phase of PZ.

Figures 9(a)–9(c) and 10(a)–10(c) illustrate the temperature dependence of the superlattice reflections. Figures 9(a)–9(c) show the ⟨001⟩ SAED patterns at temperatures of 300, 200, and 20, respectively. Figures 10(a)–10(c) show the ⟨112⟩ SAED patterns at 20, −15, and −75 °C, respectively. At 300 °C [Fig. 9(a)], weak diffuse $\frac{1}{2}\langle 110\rangle$ superlattice reflections were observed (as arrowed), indicating the presence of a soft M_3 oxygen rotational mode. However, no weak diffuse $\frac{1}{2}\langle 111\rangle$ superlattice reflections were found to coexist with the $\frac{1}{2}\langle 110\rangle$ reflections in the ⟨112⟩ SAED pattern (data not shown) in this temperature range as for PZ [see Fig. 1(e)], indicating the absence of a soft Γ_{25} mode. On cooling through the paraelectric-ferroelectric transformation (∼245 °C), the diffuse $\frac{1}{2}\langle 110\rangle$ reflections were observed to sharpen [Fig. 9(b)]. These results show that the condensation of a zone-center phonon mode (Γ_{15}) is related to an ordering of M-type oxygen rotations. At temperatures between 200 and 20 °C, no significant changes were observed in the SAED patterns [Figs. 9(b) and 9(c)]. However, the presence of a splitting of the $\frac{1}{2}\langle 110\rangle$ reflections should be noted in Figs. 9(b) and 9(c), as indicated by arrows.

On cooling between 20 and −15 °C, the intensity of the $\frac{1}{2}\langle 110\rangle$ superlattice reflections decreased, and the presence of $\frac{1}{2}\langle 111\rangle$ superlattice reflections became evident [Figs. 10(a) and 10(b)]. These results indicate that the Γ_{25} rotational modes soften in this temperature range and consequently M-type and R-type oxygen rotations coexist. On further cooling to −75 °C [Fig. 10(c)], strong $\frac{1}{2}\langle 111\rangle$ superlattice reflections were observed, however the $\frac{1}{2}\langle 110\rangle$ superlattice reflections disappeared. These results are indicative of a diffuse oxygen rotational transformation between M-type and R-type tilts. No such transformation was observed in PZ, rather the coexistence of both rotational systems was found to high temperatures. The diffuseness of this transformation for PZT 95/5 may reflect a difficulty in developing new ordered rotations in a rigid oxygen framework. Accompanying this diffuse transformation from M-type to R-type tilts, a gradual FE to AFE transformation was observed on cooling. Figures 11(a) and 11(b) show ⟨001⟩ SAED patterns at 25 and −90 °C, respectively. $\frac{1}{2}\langle 110\rangle$ superlattice reflections are evident at 25 °C which are indicative of a FE state. On cooling to −90 °C, $\frac{1}{4}\langle 110\rangle$ superlattice reflections were found clearly indicating that the low-temperature case is AFE$_O$ and isostructural with that of

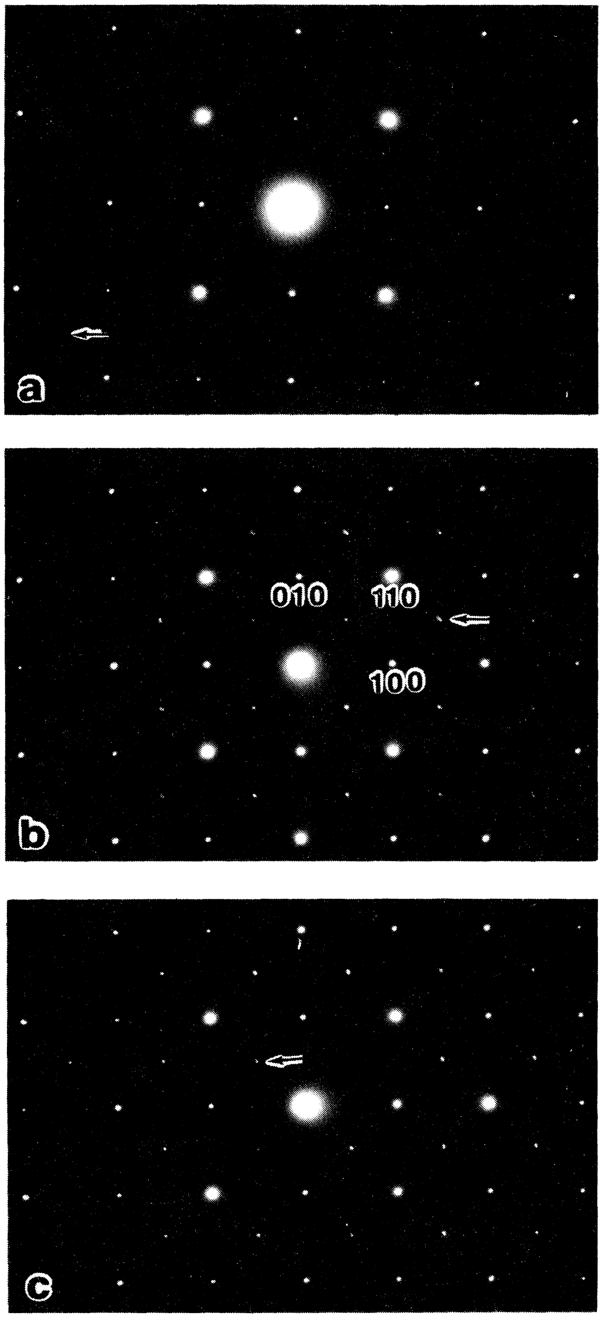

FIG. 9. ⟨001⟩ SAED patterns of PZT 95/5 on cooling at various temperatures. (a) 300 °C, (b) 200 °C, and (c) 20 °C.

PZ. It would appear that the sequence and coexistence of oxygen rotations which occurs with decreasing temperature is changed with increasing Ti content between PZ and PZT 95/5. These changes may be, in part, responsible for the observed rapid changes in the relative phase stabilities of the ferroelectric and antiferroelectric phases in the high Zr content end of the PZT crystalline solution series.

To identify the symmetry of the ferroelectric phase of PZT 95/5, CBED studies were performed. A [001] zone axis CBED pattern for PZT 95/5 taken at room temperature is shown in Fig. 12. Similar symmetries can be seen as observed in the intermediate phase region for PZ [Fig. 8(c)] and rhombohedral PZT 65/35 [Fig. 8(d)]. In this pattern, a single mirror plane can be seen which is parallel to the [110]. These results clearly show that the ferroelectric state for PZT 95/5 has rhombohedral symmetry.

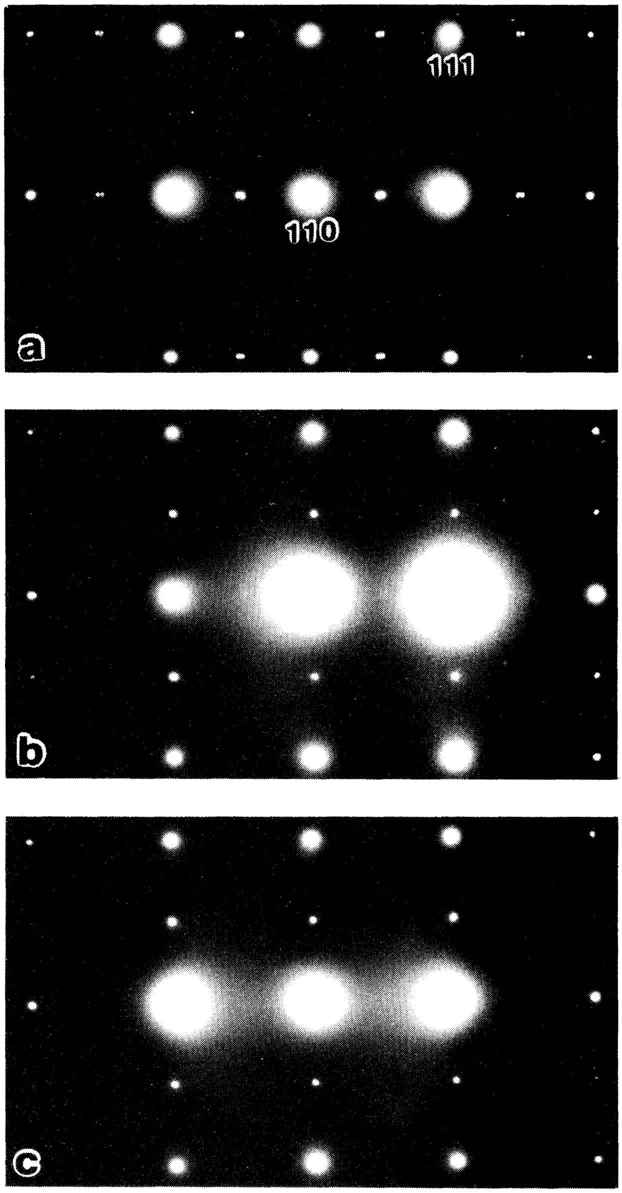

FIG. 10. ⟨112⟩ SAED patterns of PZT 95/5 on cooling at various temperatures. (a) 20 °C, (b) −15 °C, and (c) −75 °C.

2. *Lattice imaging of ⟨110⟩ structural modulations*

Splitting of the $\frac{1}{2}\langle 110\rangle$ superlattice reflections was evident in the ⟨112⟩ SAED pattern given in Fig. 10(a). Splitting in the ⟨001⟩ and ⟨110⟩ SAED patterns was

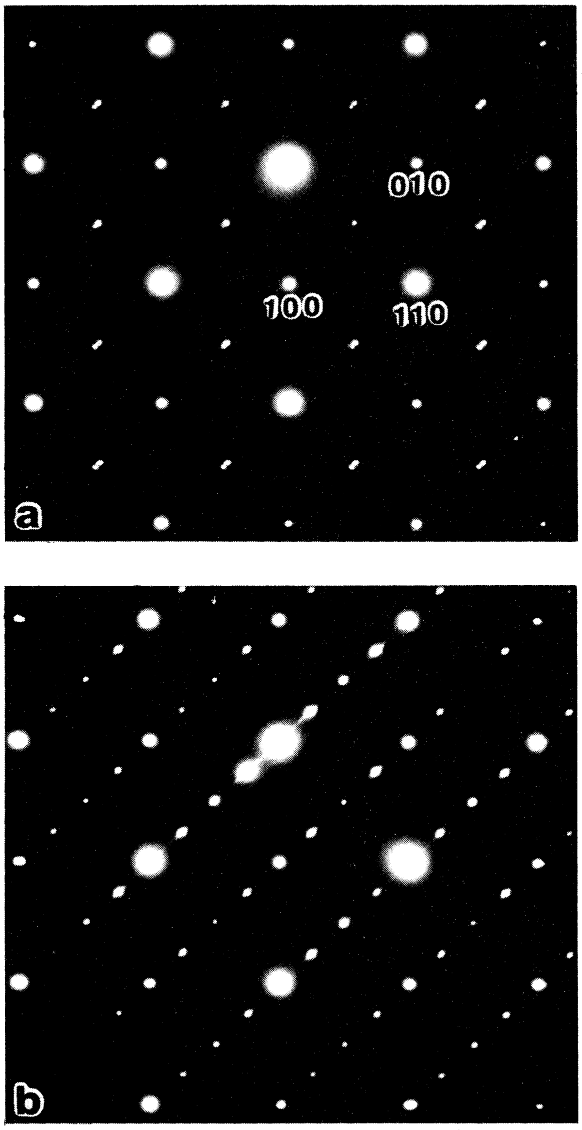

FIG. 11. ⟨001⟩ SAED pattern of PZT 95/5 at −90 °C.

also observed [Figs. 8(c) and 8(d)]. This splitting is indicative of the existence of a domain structure associated with the $\frac{1}{2}\langle 110\rangle$ reflections. However, the SAED patterns were not taken from a region covering two ferroelectric domains. These results are suggestive of a subdomain structure within the ferroelectric domains. In consideration that the $\frac{1}{2}\langle 110\rangle$ reflections results from a soft M_3 oxygen rotational mode, the spitting of the reflections may arise from domain regions with variously oriented M-type oxygen octahedron tilts.

Lattice imaging revealed the presence of nanosized domain regions which contained variously oriented ⟨110⟩ structural modulations. Figure 13(a) shows a high-resolution lattice image for PZT 95/5 taken at room temperature. A corresponding ⟨111⟩ SAED pattern is given in Fig. 13(b), which was obtained using a diffraction aperture size of 1 μm. The ⟨111⟩ SAED pattern reveals $\frac{1}{2}\langle 110\rangle$ superlattice reflections along the [110], [011], and [101] axes. This indicates that the modulated structure seems to be three-dimensional, having an average rhombohedral symmetry as shown by CBED. However, the lattice image shown in Fig. 13(a) clearly reveals a one-dimensionality in the ⟨110⟩ structural modulations, where the unit cell is doubled along the ⟨110⟩. Nanosized domain regions, ~10 nm in size, can clearly be seen which contain ⟨110⟩ structural modulations [regions A, B, and C in Fig. 13(a)]. Some regions of the specimen did not show any ⟨110⟩ structural modulations, as indicated by region D. The orientation of the structural modulation can be seen to change between domain regions. The arrows are shown in this figure to indicate the orientations of the structural modulations within three different nanosized domain regions. Figure 13(c) shows an optical diffraction pattern obtained by using a laser beam to cover the nanosized domain region A in the corresponding negative. This region had only a single one-dimensional modulation. This figure clearly shows only one set of $\frac{1}{2}\langle 110\rangle$ superlattice reflections. The optical diffraction pattern shown in Fig. 13(d) was obtained from a larger area which contained multiple modulations. This figure reveals three sets of $\frac{1}{2}\langle 110\rangle$ reflections, similar to the ⟨111⟩ SAED pattern shown in Fig. 13(b). The presence of multiple orientations of the structural modulations on a small scale is consistent with the observed average rhombohedral symmetry, as determined by CBED which obtained from an area greater than 40 nm in size.

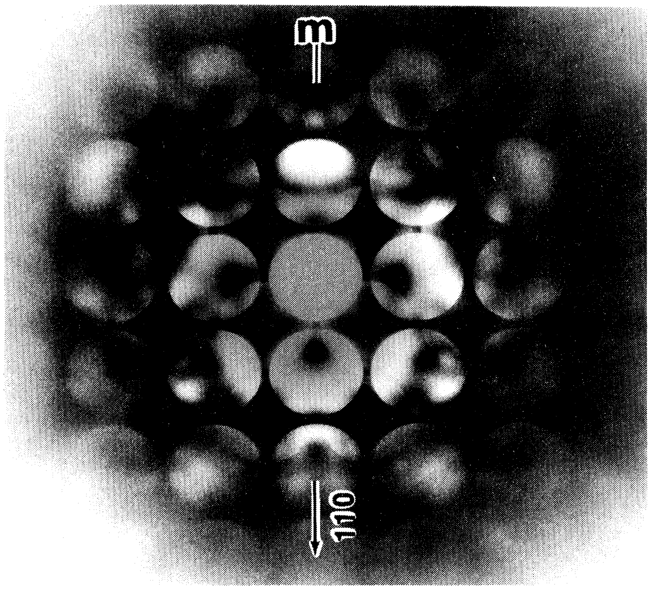

FIG. 12. [001] zone-axis convergent beam electron-diffraction pattern at room temperature for PZT 95/5.

Figure 13(a) was shown to illustrate the one-dimensionality of the ordered structure and the size of the ordered domains. The observed contrast in the lattice

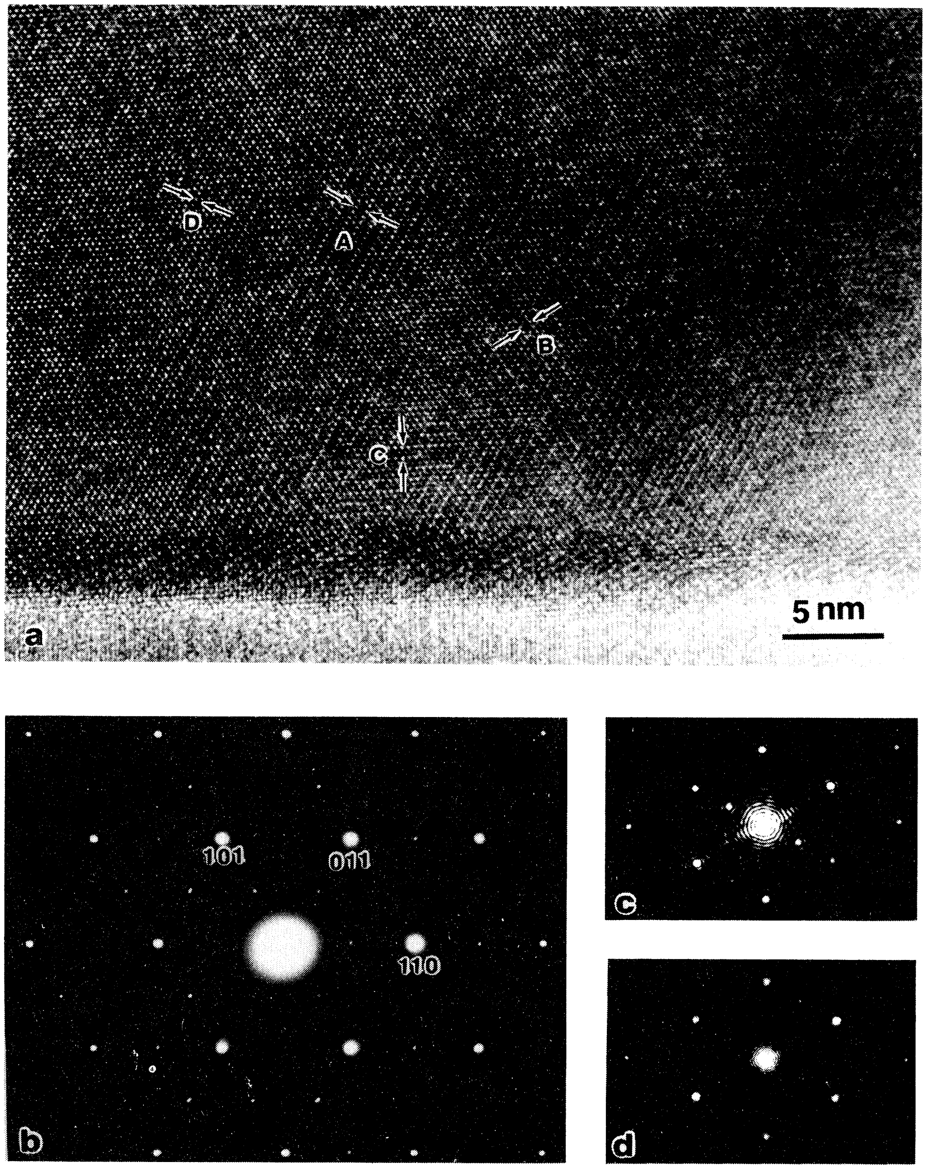

FIG. 13. Structural modulations at room temperature in PZT 95/5. (a) ⟨111⟩ lattice image, (b) ⟨111⟩ selected area electron-diffraction pattern, (c) optical diffraction pattern taken from an area covering a single modulation, and (d) optical diffraction pattern taken from an area covering multiple structural modulations.

image may be due to a coupling of the oxygen rotations to the polarization. Rotostrictive couplings to the polarization are well known,[31] which result in a tilting of the polarization as the oxygen octahedron rotate.[31–33] The results presented in this study indicate the existence of a hierarchy of symmetries in the $\mathrm{FE}_{R[HT]}$ state of PZT 95/5. The symmetry due to the cation displacements is rhombohedral due to a long-range ordering of Zr and Ti ion displacements along ⟨111⟩ arising from the softening of the Γ_{15} mode, however the local symmetry due to oxygen octahedral rotations may be tetragonal due to the soft M_3 oxygen rotational mode. Macroscopic rhombohedral symmetry can be preserved by averaging in over many small ordered regions with ⟨110⟩ structural modulations.

C. $\mathrm{Pb(Zr_{0.90}Ti_{0.10})O_3}$ and $\mathrm{Pb(Zr_{0.80}Ti_{0.20})O_3}$

TEM investigations were also performed for higher Ti content specimens. Figures 14(a) and 14(b) show room-temperature ⟨001⟩ and ⟨110⟩ SAED patterns for PZT 90/10, and Figs. 14(d) and 14(e) show ⟨001⟩ and ⟨110⟩ SAED patterns for PZT 80/20, respectively. For PZT 90/10, weak diffuse $\frac{1}{2}\langle 110\rangle$ superlattice reflections were observed, as indicated by an arrow in Fig. 14(a). In addition, strong $\frac{1}{2}\langle 111\rangle$ reflections are clearly evident in Fig. 14(b). These results indicate the presence of locally ordered M-type oxygen tilts. These locally ordered M-type tilts coexist with ordered R-type tilt domains. Figure 14(c) is a bright-field image for PZT 90/10 showing typical ferroelectric domains. The existence of $\frac{1}{2}\langle 111\rangle$ su-

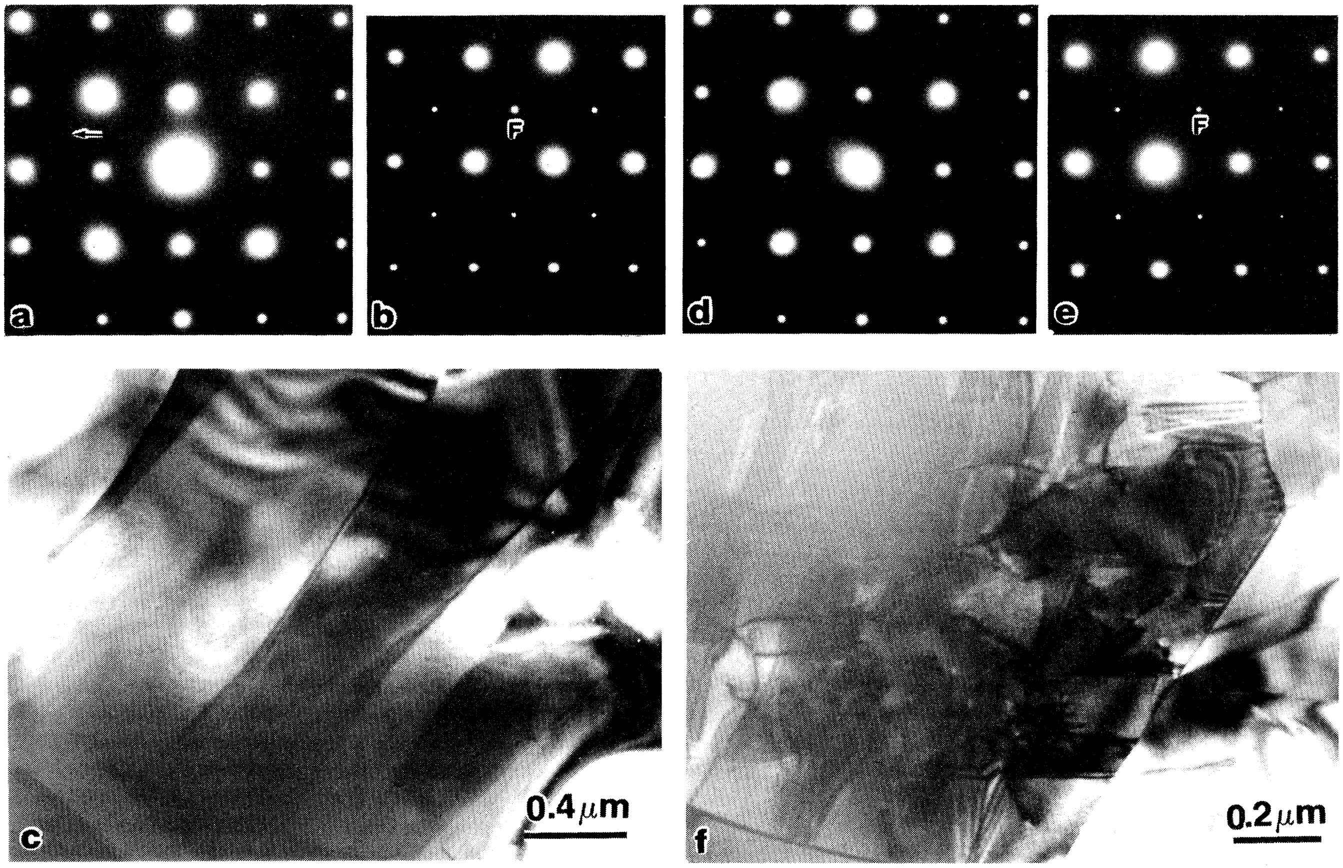

FIG. 14. Room-temperature TEM results for various PZT compositions. (a) ⟨001⟩ SAED pattern for 90/10, (b) ⟨110⟩ SAED pattern for 90/10, and (c) bright-field image for 90/10, (d) ⟨001⟩ SAED pattern for 80/20, (e) ⟨110⟩ SAED pattern for 80/20, and (f) bright-field image for 80/20.

perlattice reflections shows that the phase is the low-temperature rhombohedral ferroelectric. These results indicate the existence of a hierarchy of domain states for PZT 90/10. Ferroelectric rhombohedral domains exist which contain ordered *R*-type tilt domains. The ordered *R*-type tilt domains then coexist with locally ordered *M*-type oxygen rotations. Hot-stage TEM studies revealed a transition between *R*-type and *M*-type oxygen rotational systems on heating (data not shown). For PZT 90/10, the high-temperature rhombohedral ferroelectric phase was found to be characterized by $\frac{1}{2}\langle 001 \rangle$ superlattice reflections.

For PZT 80/20, no $\frac{1}{2}\langle 110 \rangle$ superlattice reflections were visible in the ⟨001⟩ SAED pattern, as shown in Fig. 14(d), and extended long exposure only revealed very weak diffuse $\frac{1}{2}\langle 110 \rangle$ superlattice reflections. However, strong $\frac{1}{2}\langle 111 \rangle$ superlattice reflections were observed in the ⟨110⟩ pattern shown in Fig. 14(e). These results indicate that PZT 80/20 is in the low-temperature rhombohedral ferroelectric state at room temperature. A bright-field image is shown in Fig. 14(f). This image reveals typical rhombohedral ferroelectric domains. Hot-stage TEM studies revealed that the $\frac{1}{2}\langle 111 \rangle$ reflections disappeared on heating near 150 °C. No evidence of any distinct $\frac{1}{2}\langle 110 \rangle$ superlattice reflections was found above the transformation temperature and upon further heating to 300 °C. These results are clearly different than those found for PZT 95/5 [see Figs. 9(a)–9(c) and 10(a)–10(d)], which revealed a transition between *R*-type and *M*-type tilt structures with temperature. No evidence of any ordered or locally ordered tilt structure was found in the high-temperature rhombohedral ferroelectric state for PZT 80/20. The *M*-type tilt structure would seemingly slowly weaken with increasing Ti content above ~ 10 at. %.

V. PHASE DIAGRAM

The results of this investigation are summarized in the phase diagram given in Fig. 15. Dots are used to represent *M*-type oxygen tilts and dashed lines represent *R* type. The degree of oxygen octahedral ordering is qualitatively represented by the density of dots and dashed lines. Locally ordered *M*-type and *R*-type oxygen tilt structures are shown to coexist to high temperatures for PZ and the PZT crystalline solutions ($x < 0.05$). On

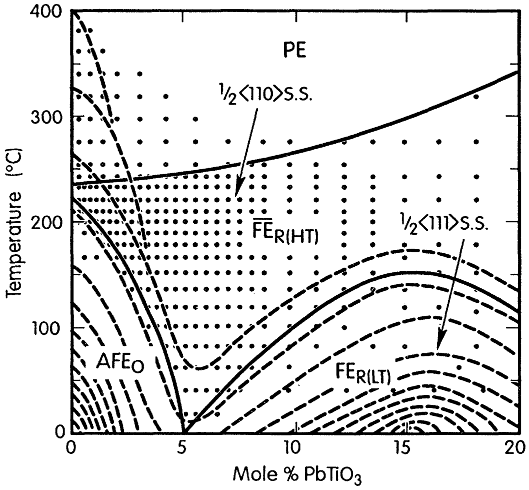

FIG. 15. Revised phase diagram for high zirconium content PZT. The densities of spots and dashed lines are qualitatively proportional to the intensity of superlattice reflections and to the degree of ordering in the oxygen octahedral rotations. The overlap of spots and dashed lines indicates the coexistence of both M- and R-type oxygen octahedral rotations. Solid lines are used to denote phase boundaries between ferroelectric, antiferroelectric, and paraelectric states. The term SS is used to designate the term superlattice spot.

decreasing temperature, these tilt structures are both shown to order at the transformation temperature into an intermediate ferroelectric state with rhombohedral symmetry. This phase region is shown in the phase diagram as $\overline{\text{FE}}_{R(HT)}$ (with M- and R-type ordered tilts). The notation $\overline{\text{FE}}_{R(HT)}$ is used to indicate a local tetragonal symmetry in the oxygen framework (due to oxygen octahedral rotations) within the global rhombohedral symmetry. On further cooling, a transformation to the AFE$_O$ state occurred. This region is shown in the phase diagram as AFE$_O$ (with R-type ordered tilts).

With increasing Ti content ($0.03 \leq x \leq 0.05$), no locally ordered R-type tilt structures were observed at high temperatures in the paraelectric state. Rather, only locally ordered M-type rotations were found. With decreasing temperature, a transformation into a $\overline{\text{FE}}_{R(HT)}$ state is shown in the phase diagram. This phase region was characterized by $\frac{1}{2}\langle 110 \rangle$ reflections. The temperature stability range of the $\overline{\text{FE}}_{R(HT)}$ state is shown to be significantly enhanced with respect to that of PZ. On further cooling to below room temperature, a transformation to an AFE$_O$ state is shown. At this transformation, a transition between ordered M-type and R-type oxygen tilts is also shown.

Hot-stage TEM studies revealed that the ferroelectric phase for 90/10 was characterized by $\frac{1}{2}\langle 110 \rangle$ reflections, i.e., $\overline{\text{FE}}_{R(HT)}$. With a further increase in the Ti content ($x > 0.15$), only locally ordered M-type tilt structures were found in the ferroelectric state. No ordered M-type oxygen rotations were observed. With a decrease in the temperature, ordered R-type oxygens rotations developed for both 90/10 and 80/20. This region is shown in the phase diagram as FE$_{R(LT)}$ (with R-type ordered tilts). With increasing Ti content, the locally ordered M-type tilt structures were weakened, however it is not known how far over into the Ti-rich side of the phase diagram they extend. SAED patterns only revealed very weak diffuse $\frac{1}{2}\langle 110 \rangle$ superlattice reflections for $x = 0.20$ by extended long exposure. Clearly, a hierarchy of symmetries (and domain structures) exists over a wide region of the rhombohedral ferroelectric phase field.

VI. CONCLUSIONS

TEM studies have been performed on a series of high Zr content PZT compositions. These studies have revealed several new and important findings. First, the existence of locally ordered R-type and M-type oxygen rotations were found in the cubic phase. On transformation to an intermediate phase region between the AFE$_O$ and PE states, an ordering of oxygen rotations was observed. Second, hot-stage TEM investigations have revealed for the first time the presence of ferroelectric domains in the intermediate phase region. These results in conjunction with CBED patterns showed that the intermediate state is rhombohedral ferroelectric. This rhombohedral ferroelectric state ($x < 0.10$) was found to be characterized by the presence of $\frac{1}{2}[110]$ superlattice reflections, associated with ordered M-type oxygen rotations. Third, lattice imaging revealed $\langle 110 \rangle$ orientated structural modulations. The local symmetry due to the structural modulations was tetragonal. Finally, it is believed that a hierarchy of symmetries exists over a wide region of the rhomobohedral ferroelectric phase field. A modification of the high Zr content end of the Pb(Zr$_{1-x}$Ti$_x$)O$_3$ phase diagram is proposed to account for this hierarchy.

ACKNOWLEDGMENTS

This research was supported in full by the Office of Naval Research (ONR) under Contract No. N00014-92-J-1522 and by the Naval UnderSea Warfare Center in New London, CT, under Contract No. N66604-94-C-0984. The use of facilities in the Center for Microanalysis of Materials Research Laboratory at the University of Illinois at Urbana-Champaign is gratefully acknowledged.

---

[1] E. Sawaguchi, G. Shirane, and Y. Takagi, J. Phys. Soc. Jpn. **6**, 333 (1951); **7**, 110 (1950).

[2] Z. Ujma and J. Handerek, Phys. Status Solidi A **28**, 489 (1982).

[3] M. Tanaka, R. Saito, and K. Tsuzuki, J. Phys. Soc. Jpn. **51**, 2635 (1982).

[4] F. Jona, G. Shirane, F. Mazzi, and R. Pepinsky, Phys. Rev. **105**, 849 (1957).

[5] E. Sawaguchi, H. Maniwa, and S. Hoshino, Phys. Rev. **83**, 1078

(1951).

[6] H. Fujishita and S. Hashino, J. Phys. Soc. Jpn. **53**, 226 (1984).

[7] G. Shirane, E. Sawaguchi, and A. Takeda, Phys. Rev. **80**, 485 (1950).

[8] B. Jaffe, W. R. Cook, and H. Jaffe, *Piezoelectric Ceramics* (Academic, London, 1971).

[9] V. J. Tennery, J. Am. Ceram. Soc. **49**, 483 (1966).

[10] L. Goulpeau, Fiz. Tverd. Tela **8**, 2469 (1966) [Sov. Phys. Solid State **8**, 1970 (1967)].

[11] G. Shirane, E. Sawaguchi, and Y. Takagi, Phys. Rev. **84**, 476 (1951).

[12] B. A. Scott and G. Burns, J. Am. Ceram. Soc. **55**, 331 (1972).

[13] K. Roleder, G. Kugel, J. Handerek, M. D. Fontana, C. Carabatos, M. Hafid, and A. Kania, Ferroelectrics **80**, 161 (1988).

[14] C. Kittle, Phys. Rev. **82**, 729 (1951).

[15] L. E. Cross, Philos. Mag. Ser. 8, **1**, 76 (1956).

[16] W. Cochran and A. Zia, Phys. Status Solidi **25**, 273 (1968).

[17] A. M. Glazer, Acta Crystallogr. A **31**, 756 (1975).

[18] X. H. Dai, A. DiGiovanni, and D. Viehland, J. Appl. Phys. **74**, 3399 (1993).

[19] Y. Fujii, S. Hoshino, Y. Yamada, and G. Shirane, Phys. Rev. B **9**, 4549 (1974).

[20] G. Shirane and Y. Yamada, Phys. Rev. **177**, 858 (1969).

[21] R. W. Whatmore and A. M. Glazer, J. Phys. C **12**, 1505 (1979).

[22] B. Rechav, Y. Yacoby, E. A. Stern, J. J. Rehr, and M. Newville, Phys. Rev. Lett. **72**, 1352 (1994).

[23] C. Randall, D. Barber, R. Whatmore, and P. Croves, Ferroelectrics **76**, 277 (1987).

[24] A. M. Glazer and H. D. Megaw, Philos. Mag. **25**, 1119 (1972).

[25] Z. Xu, D. Viehland, P. Yang, and D. A. Payne, J. Appl. Phys. **74**, 3406 (1993).

[26] Z. Xu, X. H. Dai, and D. Viehland, Phys. Rev. B **51**, 6261 (1995).

[27] P. Yang, Ph.D. thesis, University of Illinois at Urbana-Champaign, 1992.

[28] D. Berlincourt and H. Krueger, "Research on Piezoelectric Materials and Phenomena," Clevite Report to Sandia National Laboratory, Project No. 323110, 1963.

[29] C. Randall, D. Barber, and R. Whatmore, J. Mater. Sci. **22**, 925 (1987).

[30] X. H. Dai, Z. Xu, and D. Viehland, J. Appl. Phys. **77**, 5086 (1995).

[31] M. J. Haun, Ph.D. dissertation, Pennsylvania State University, 1988.

[32] C. Michel, J. M. Moreau, G. D. Achenbach, R. Gerson, and W. J. James, Solid State Commun. **1**, 865 (1969).

[33] M. E. Lines and A. M. Glass, *Principles and Applications of Ferroelectrics and Related Materials* (Clarendon, Oxford, 1977).

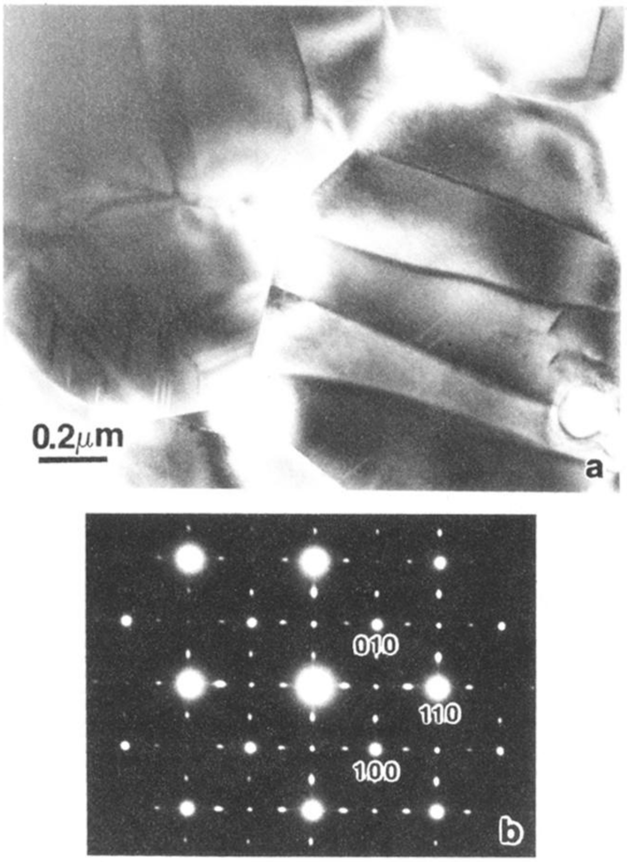

FIG. 1. Room-temperature TEM results for PZ. (a) Bright-field image, and (b) ⟨112⟩ SAED pattern.

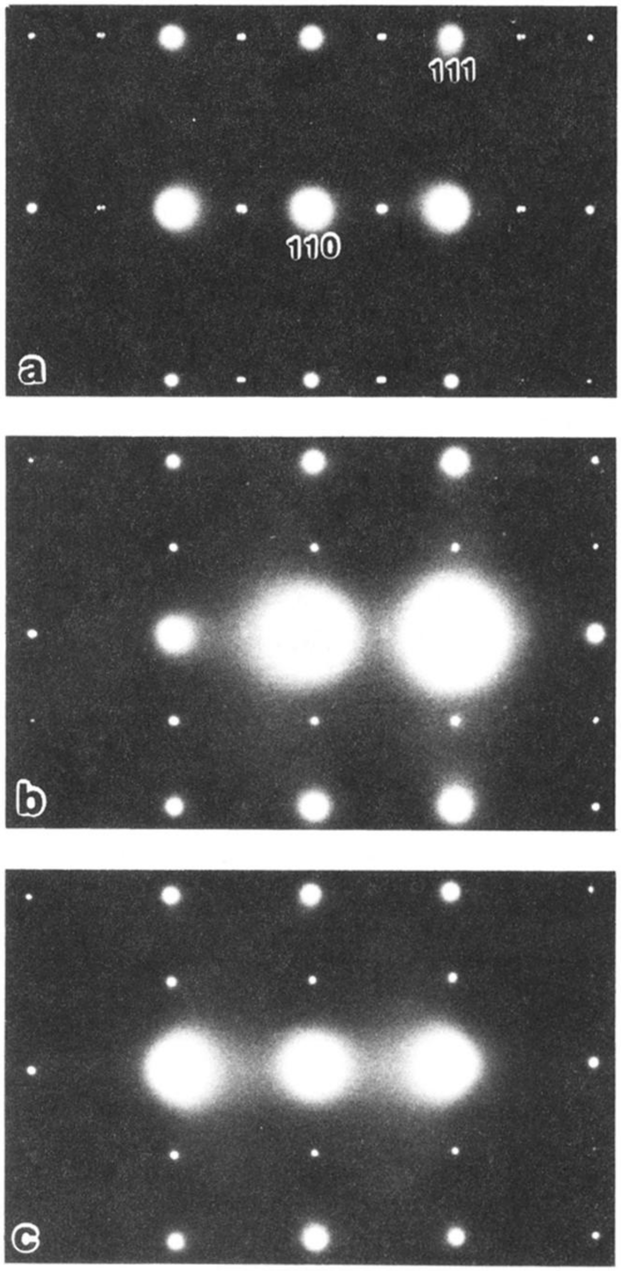

FIG. 10. ⟨112⟩ SAED patterns of PZT 95/5 on cooling at various temperatures. (a) 20 °C, (b) −15 °C, and (c) −75 °C.

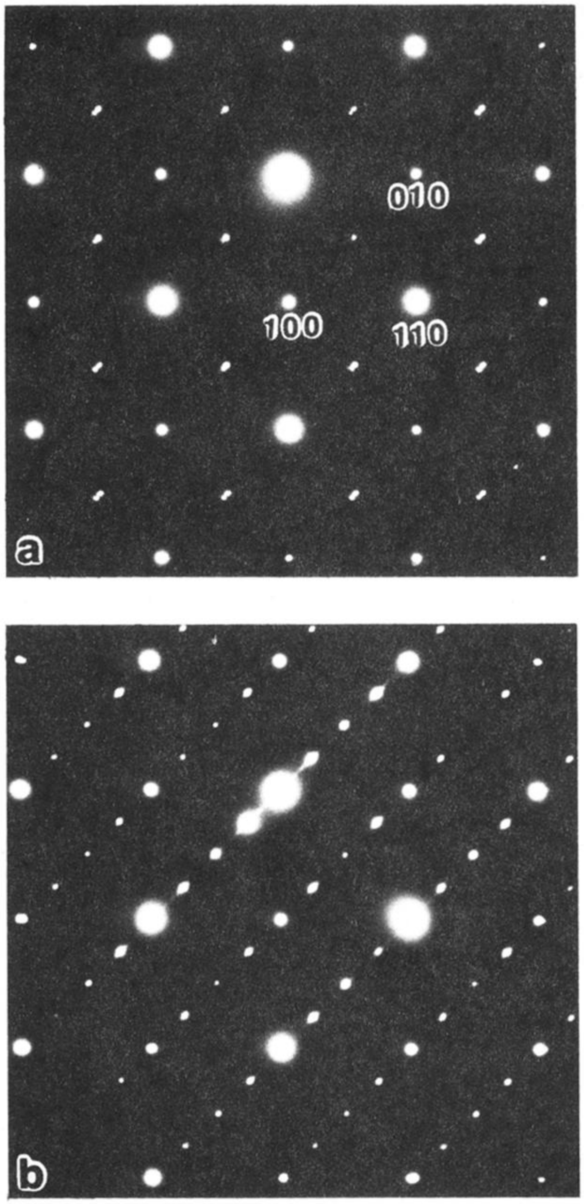

FIG. 11. ⟨001⟩ SAED pattern of PZT 95/5 at −90 °C.

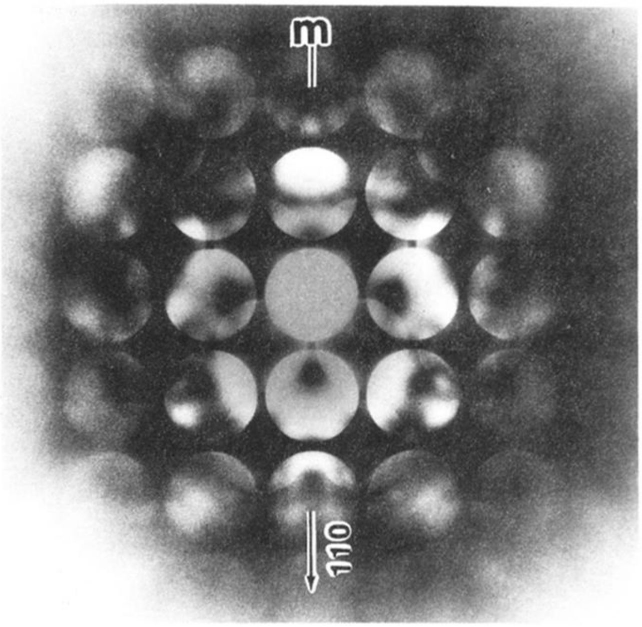

FIG. 12. [001] zone-axis convergent beam electron-diffraction pattern at room temperature for PZT 95/5.

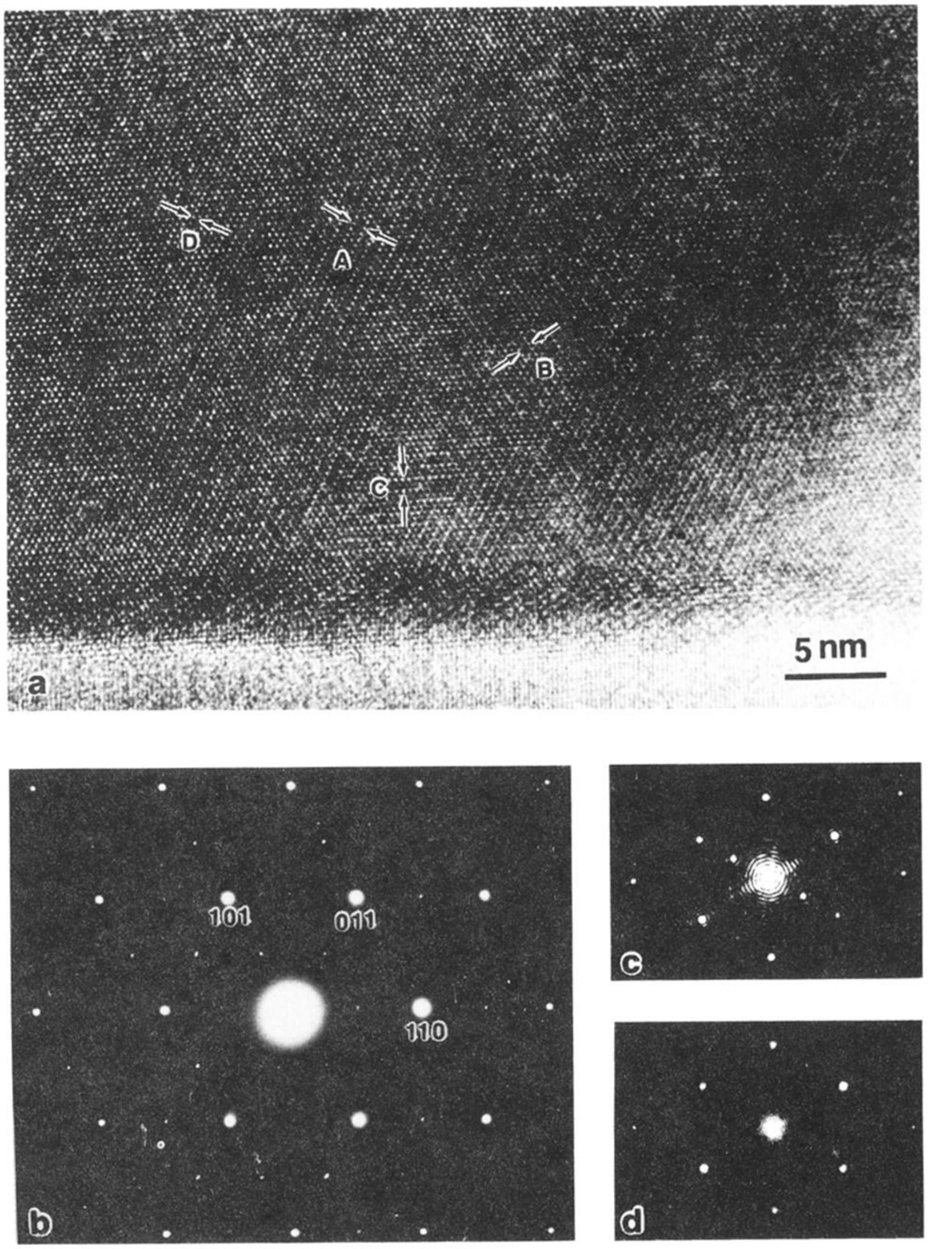

FIG. 13. Structural modulations at room temperature in PZT 95/5. (a) ⟨111⟩ lattice image, (b) ⟨111⟩ selected area electron-diffraction pattern, (c) optical diffraction pattern taken from an area covering a single modulation, and (d) optical diffraction pattern taken from an area covering multiple structural modulations.

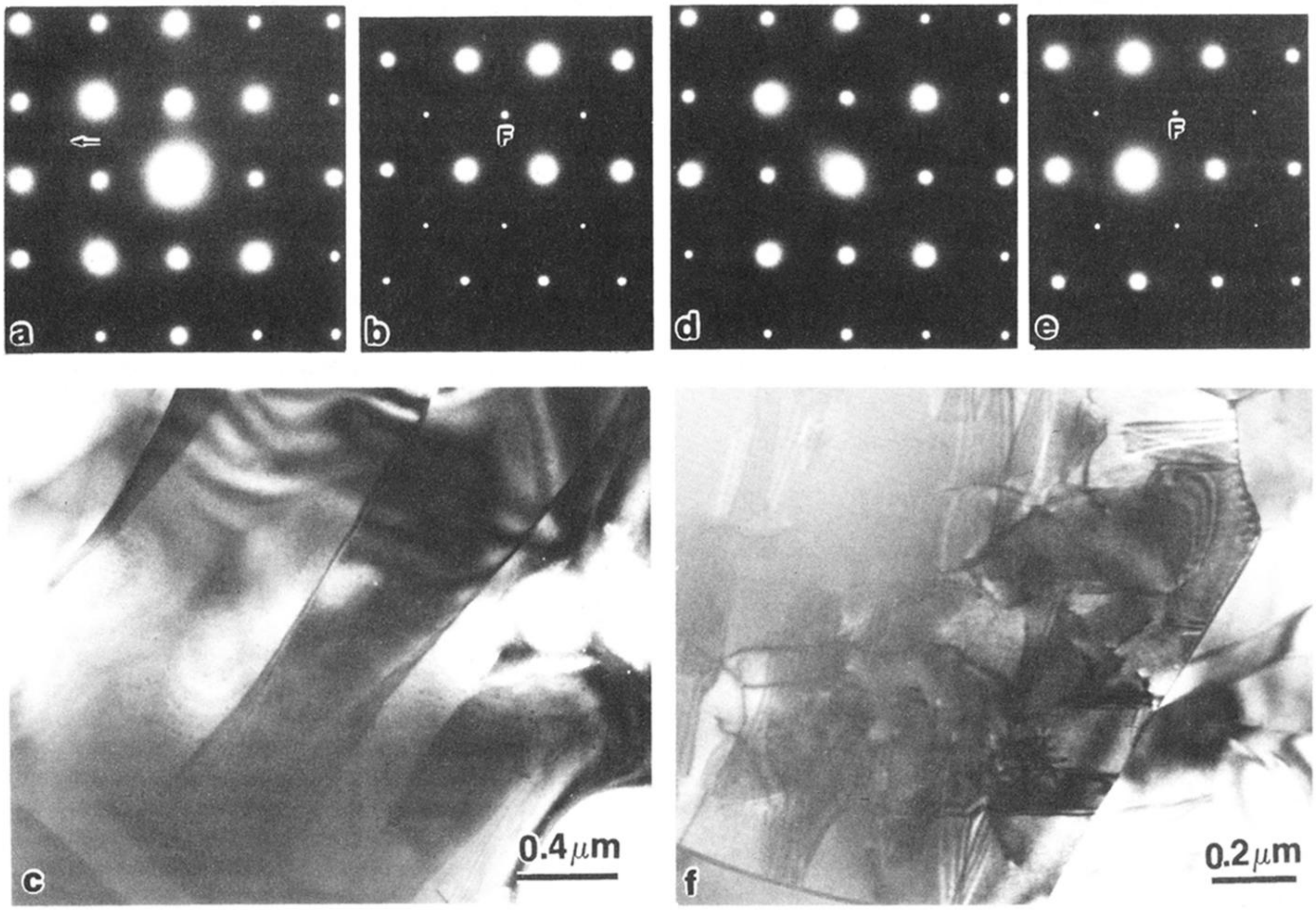

FIG. 14. Room-temperature TEM results for various PZT compositions. (a) ⟨001⟩ SAED pattern for 90/10, (b) ⟨110⟩ SAED pattern for 90/10, and (c) bright-field image for 90/10, (d) ⟨001⟩ SAED pattern for 80/20, (e) ⟨110⟩ SAED pattern for 80/20, and (f) bright-field image for 80/20.

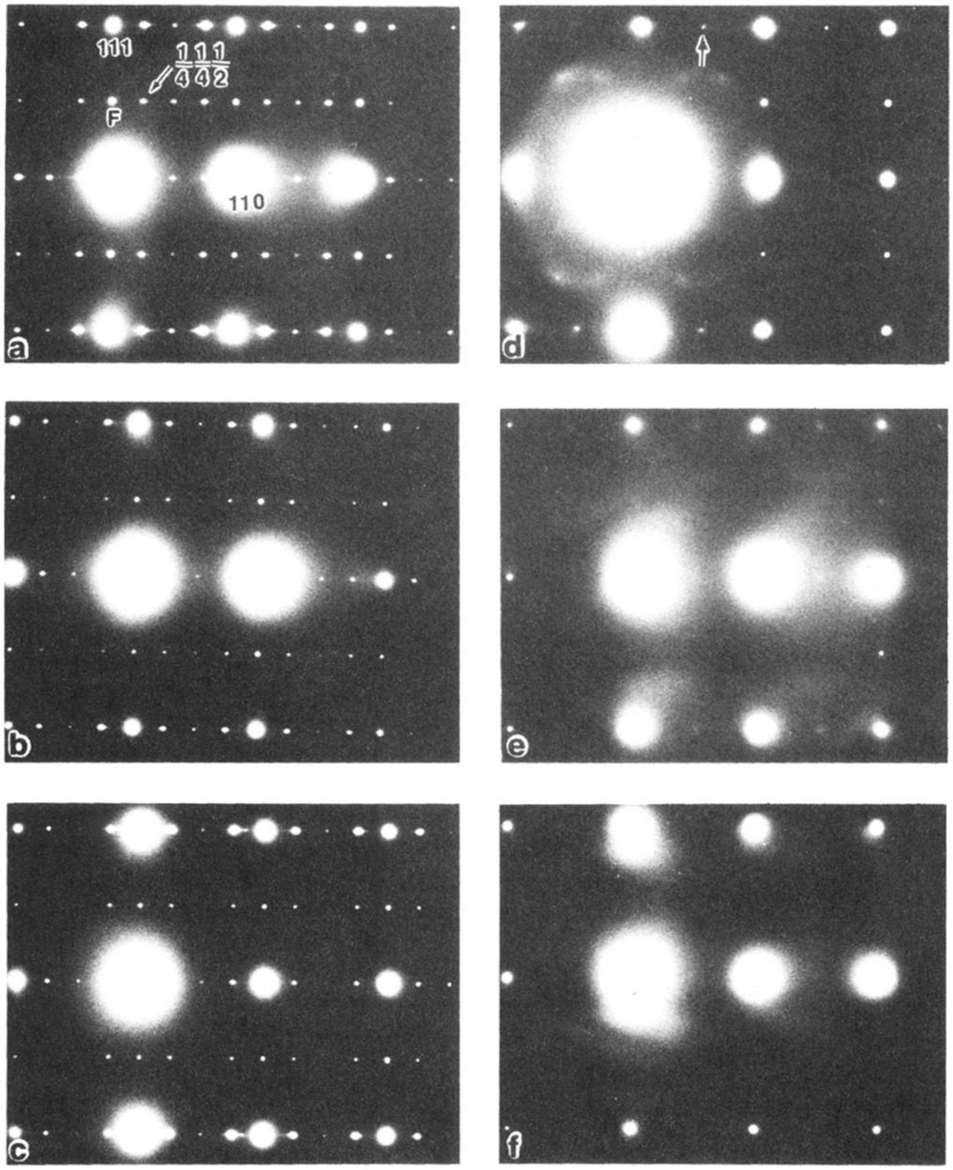

FIG. 2. ⟨112⟩ SAED patterns of PZ at temperatures (a) 20 °C, (b) 200 °C, (c) 210 °C, (d) 225 °C, (e) 320 °C, and (f) 530 °C.

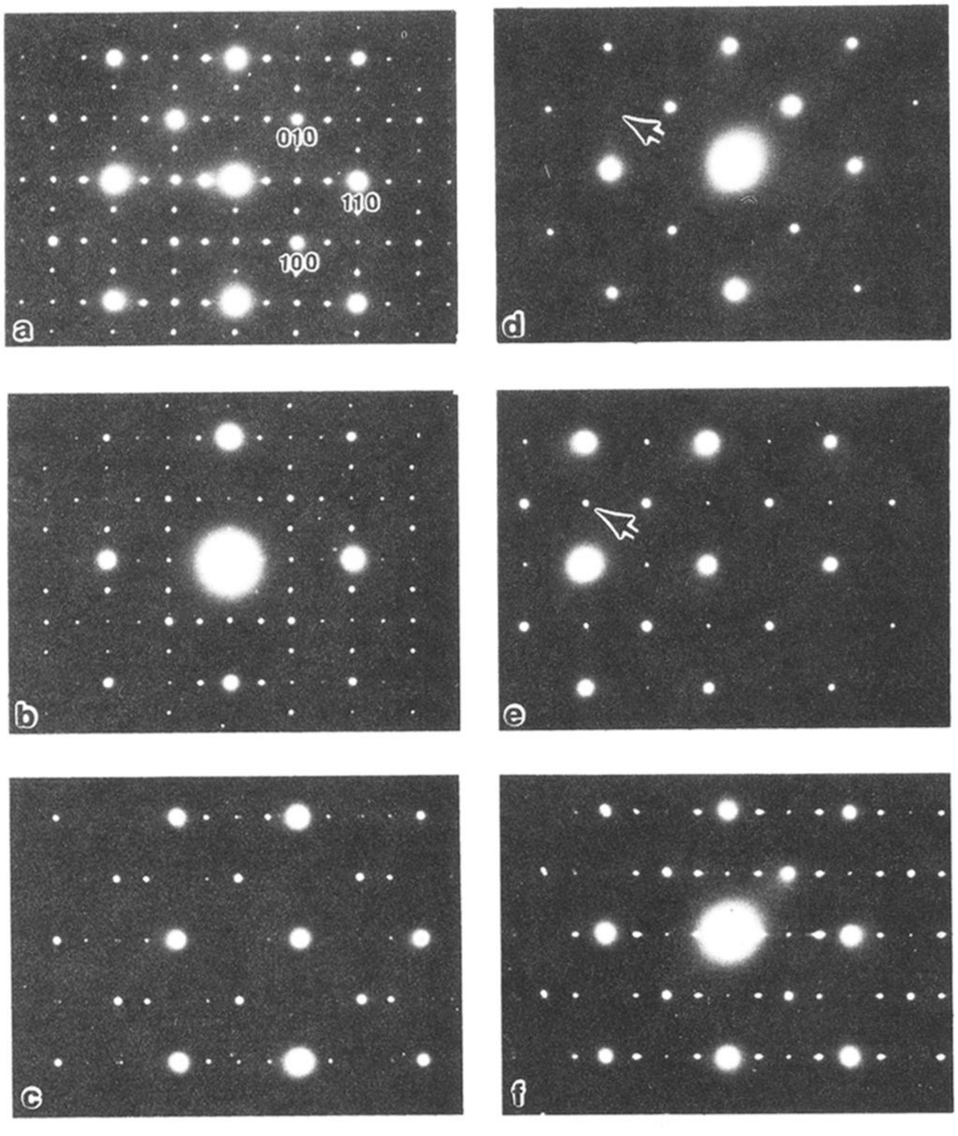

FIG. 3. ⟨001⟩ SAED patterns of PZ on heating and subsequent cooling (a) 20 °C, (b) 170 °C, (c) 220 °C, (d) 240 °C, (e) 200 °C, and (f) 20 °C.

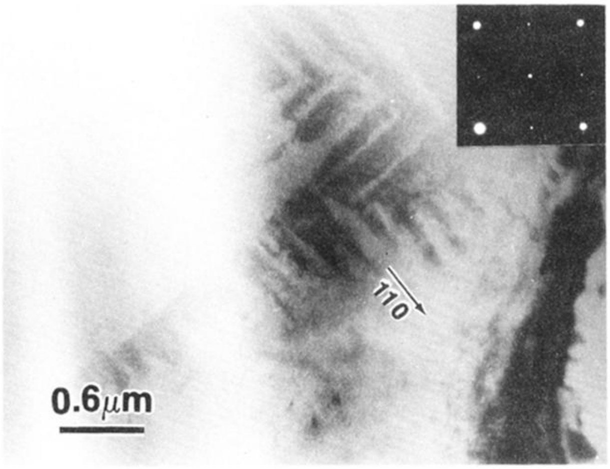

FIG. 5. Bright-field image of PZ in the intermediate phase region (225 °C).

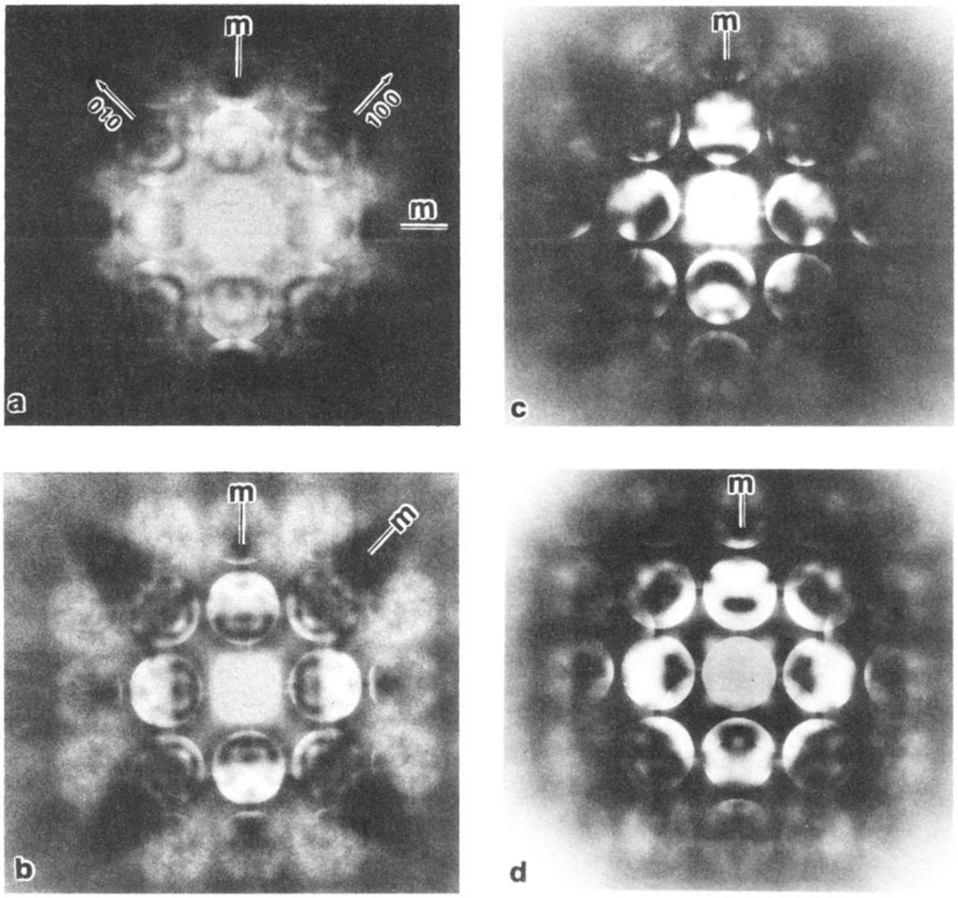

FIG. 7. [001] zone-axis convergent beam electron-diffraction patterns for PZ at various temperatures. (a) 20 °C, (b) 380 °C, (c) 200 °C, and (d) PZT 65/35 at room temperature (shown for comparisons).

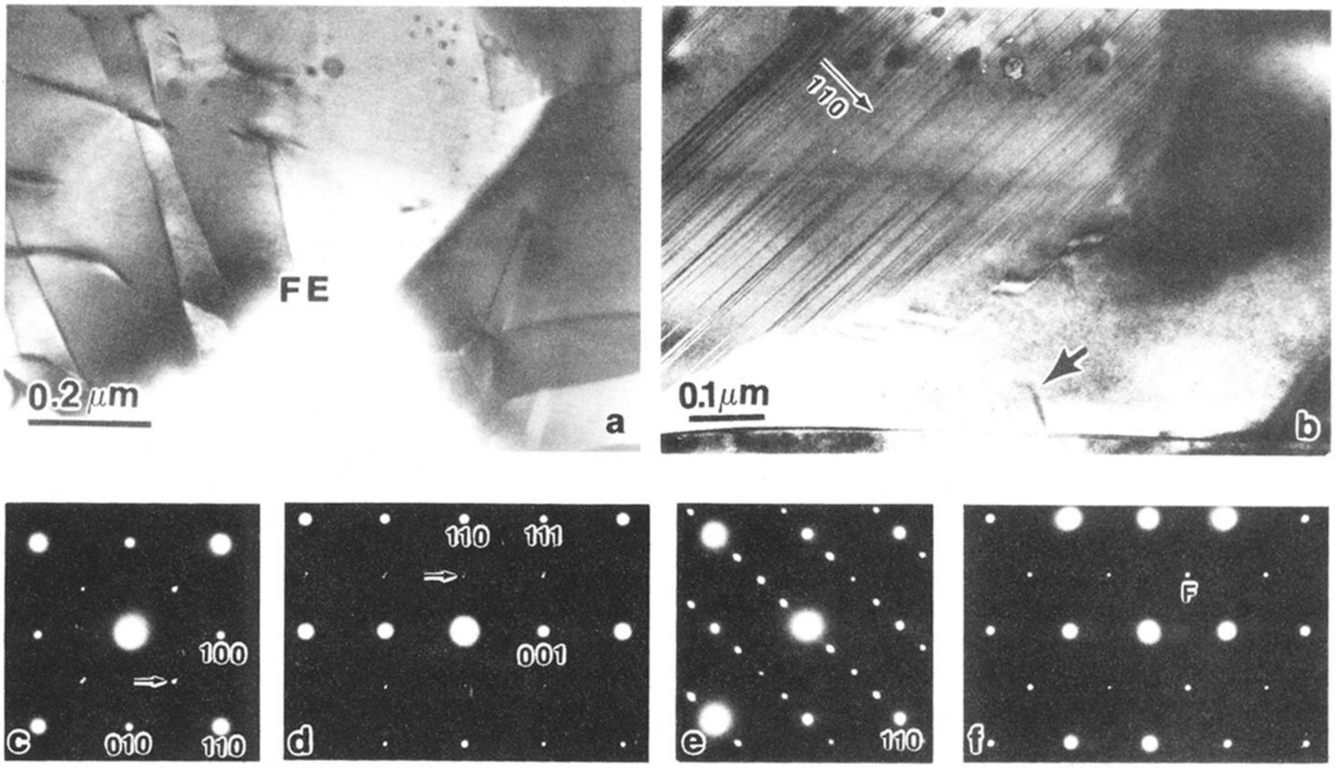

FIG. 8. Bright-field image and diffraction patterns of PZT 95/5 at 25 °C (a) dominant FE phase, (b) minor AFE phase, (c) ⟨001⟩ SAED pattern of the FE phase, (d) ⟨110⟩ SAED patterns of the FE phase, (e) ⟨001⟩ SAED pattern of the AFE phase, and (f) ⟨110⟩ SAED pattern of the AFE phase.

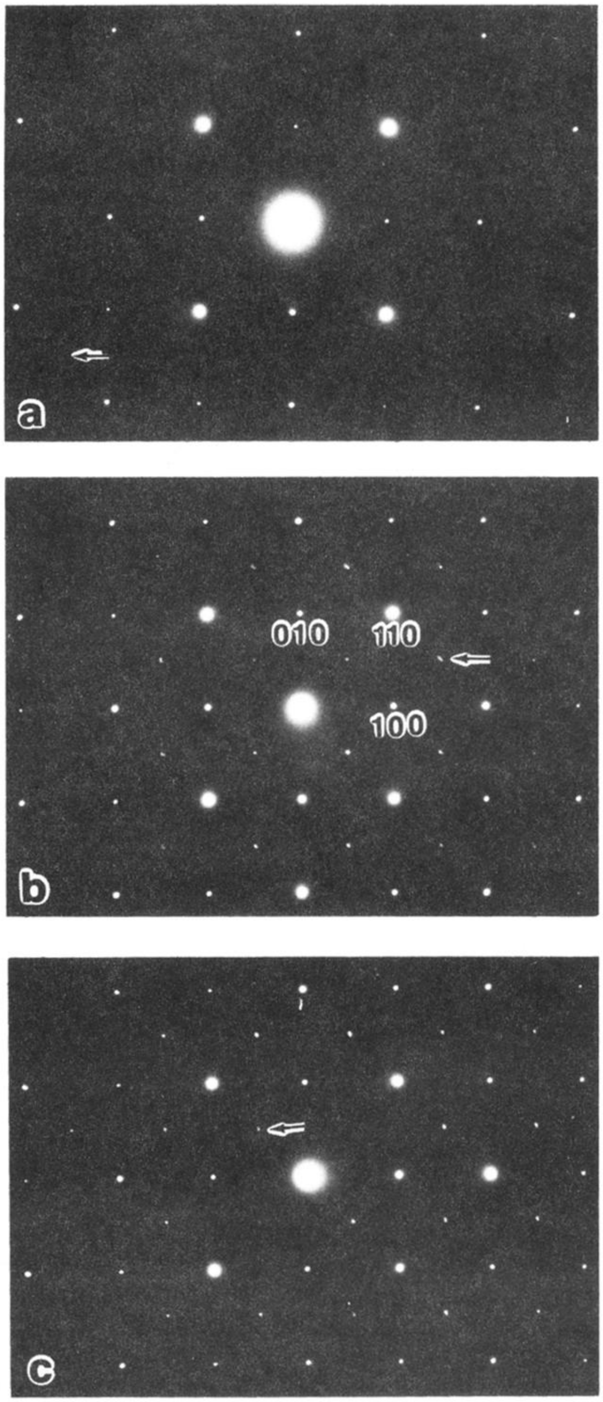

FIG. 9. ⟨001⟩ SAED patterns of PZT 95/5 on cooling at various temperatures. (a) 300 °C, (b) 200 °C, and (c) 20 °C.